

# Extraordinary March heatwave in Central Asia up to 10°C hotter in a warming climate

## Authors

Ben Clarke, *Centre for Environmental Policy, Imperial College, London, UK*

Friederike Otto, *Centre for Environmental Policy, Imperial College, London, UK*

Clair Barnes, *Centre for Environmental Policy, Imperial College, London, UK*

Maja Vahlberg, *Red Cross Red Crescent Climate Centre, The Hague, the Netherlands; Swedish Red Cross, Stockholm, Sweden (based in Umeå/Umeå, Sweden)*

## Review authors

Sjoukje Philip, *Royal Netherlands Meteorological Institute (KNMI), De Bilt, The Netherlands*

Sarah Kew, *Royal Netherlands Meteorological Institute (KNMI), De Bilt, The Netherlands*

Izidine Pinto, *Royal Netherlands Meteorological Institute (KNMI), De Bilt, The Netherlands*

Roop Singh, *Red Cross Red Crescent Climate Centre, The Hague, The Netherlands (based in New Jersey, USA)*

Emmanuel Raju, *Copenhagen Centre for Disaster Research, Global Health Section, Department of Public Health, University of Copenhagen, Copenhagen, Denmark; African Centre for Disaster Studies, North-West University, South Africa*

Nick Baumgart, *Copenhagen Centre for Disaster Research, Global Health Section, Department of Public Health, University of Copenhagen, Copenhagen, Denmark*

## Main findings

- Agriculture contributes 5-24% of GDP for the countries affected by the heatwave, and up to 50% of the workforce. Extreme heat affects agricultural workers disproportionately, reducing labor capacity, with over 230 million hours lost in Uzbekistan in 2023. The extreme temperatures this year also coincided with the flowering of key export fruit crops and sowing of spring wheat in Kazakhstan, which may impact yields.
- Central Asian countries are heavily dependent on glacier-fed irrigation systems, adding an additional layer of sensitivity, as altered snowmelt timing reduces water availability during the peak growing season.
- The study region has a very strong seasonal cycle with very hot summers and cold winters. March temperatures can therefore be very variable but temperatures as high as observed this year have in many places never been observed before. In today's climate however, which globally has warmed by 1.3 °C, the 5-day maximum and minimum temperatures observed in 2025 in the study region are not unusual with a return time of about once every 3 years.
- In a 1.3C colder climate such temperatures would however have been extremely unlikely to occur. Similarly, a 1 in 3 year March heat event would have been 5 to 10 °C cooler extrapolating the observed trends back to a 1.3 °C colder climate.
- When combining the observation-based analysis with climate models, to quantify the role of climate change in this 5-day heat event, we find that climate models underestimate the increase in heat found in observations. In particular, all observations show a particular increase in March maximum and minimum temperatures in recent years that is much stronger than in all other months, and not represented in the climate models.
- We can thus only give a conservative estimate of the influence of human-induced climate change. Based on the combined analysis we conclude that climate change made the extreme heat about 4 °C hotter and about 3 times more likely.
- Due to the known deficiencies in climate models to represent early extreme heat, estimating future changes in the 5-day maximum and minimum heat over the Central Asian region also only allows us to give very conservative estimates. At a global warming of 2.6 °C the likelihood and intensity of such events continue to increase, at least doubling in likelihood and increasing by a further 2 °C in intensity.
- Adaptation measures in the region include adjusting planting calendars, using heat-tolerant crops, and investing in resilient irrigation. Implementation varies, especially for smallholder farmers, due to resource disparities. While Kazakhstan and Tajikistan have integrated adaptation into national frameworks, and Kyrgyzstan and Tajikistan have Early Action Protocols for heat, the alarming rate of temperature increase in the region calls for an increased focus on adapting to extreme heat in the region.
- Comprehensive adaptation to heat includes adaptation at all levels such as individual self-protective behavior and heat education (e.g. first aid for heat illness), city and systems level adaptation (e.g. urban planning that includes nature based solutions, Heat Action Plans, Early Warning Systems, health-system strengthening), and national level adaptation (e.g. disaster and climate change laws that include heat, national adaptation plans, social protection systems).

## 1 Introduction

In March 2025, Central Asia experienced an unusually intense heatwave, with temperatures reaching record highs for March across the region. Countries just east of the Ural Mountains were particularly affected, setting new local records for both minimum and maximum temperatures. Especially from the 18 to the 22nd of March 2025 Kazakhstan, eastern Uzbekistan, and Turkmenistan endured the most extreme heat, while the low-lying areas of Tajikistan and Kyrgyzstan also faced unusually high temperatures. The heat event was associated with an anomalous anticyclonic circulation over the region. Generally, heatwaves are often associated with high-pressure systems, known as anticyclones, that trap warm air over the region. These systems prevent the normal movement of air, leading to stagnant, hot weather for extended periods ([Luo & Lau, 2017](#), [Yu et. al., 2019](#)).

The region is characterized by strong seasonal cycles, with summers typically very hot from May to August. However, March is generally much cooler in comparison. The early onset of such extreme heat took many by surprise, as the region is not accustomed to such temperatures at this time of year. Although the full extent of the impacts has not yet been reported, early heat waves are known to have significant effects, as communities are often unprepared for such conditions so early in the season.

The heatwave threatens public health, infrastructure, and climate-sensitive sectors like agriculture and energy. Vulnerabilities are high due to energy and water intensity, glacier retreat, and desertification, particularly in Kazakhstan, Turkmenistan, and Uzbekistan. Urban areas, including Bishkek and Tashkent, face rising heat exposure from rapid expansion, limited green space, and fragmented adaptation efforts. Rural and mountainous areas are highly vulnerable due to fragile infrastructure and dependence

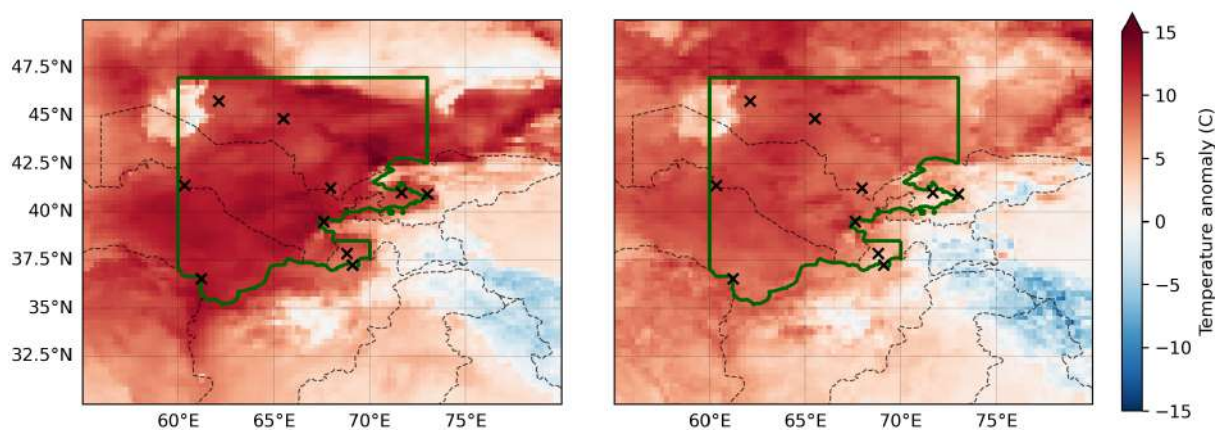


*Figure 1.1<sup>1</sup>: Anomalies of the maximum (left) and minimum (right) temperatures over Central Asia, during 18th - 22nd March 2025 versus the 1991-2020 climatological average for March. The study region is shown in green and the location of broken March temperature records are shown by black crosses.*

<sup>1</sup> Please note that in this figure, and all subsequent figures, borders do not imply official endorsement nor political opinion on included territories.

## 1.1 Heatwaves in western Central Asia

The [IPCC](#) reports with high confidence that heat extremes in the Western Central Asia region have not only increased, but that significant trends of rising temperatures have been unmistakably detected. In addition an increase in soil moisture drought is found with *medium confidence*. In a study focussing particularly on Central Asia, including the region analysed here [Fallah et al., 2023](#) found that from 1980 to 2014, an increase of 60 ppm in global CO<sub>2</sub> concentration is accompanied by a warming of 1.5 K over the whole region. They found observations to indicate a temperature rise of at least 5°C in some regions of Kazakhstan between 1990 and 2020, which are now categorized as "Temperate-cold deserts". Since the 1980s, a significant portion of Central Asia, previously characterized by a desert climate, has shifted about 100 kilometers northward, impacting southern Kazakhstan, northern Kyrgyzstan, and Uzbekistan. [Alizadeh et al., 2024](#) analysed the effect of rapid warming in the Arctic on extreme weather events in Western Central Asia and found an effect in addition to that of global warming alone that could explain the very strong increase in heat extremes. [Wang et al., 2023](#) analysed the role of soil moisture in extreme heat in central Asia and found that soil moisture depletion, driven by decreasing rainfall and increasing solar radiation, is the key driver of heatwaves in the region. They further found, as expected, that heatwaves are happening earlier, lasting longer and are more intense. The impact is particularly strong in the Western part of Central Asia, which also this study focuses on.

## 1.2 Event Definition

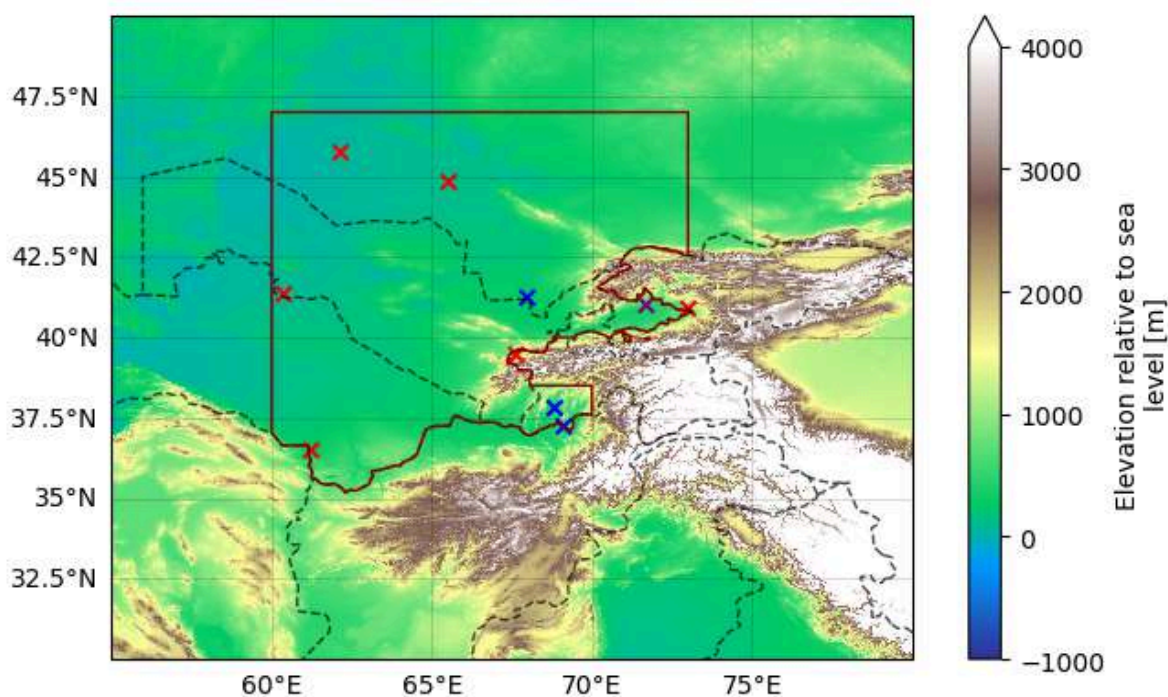


Figure 1.2: Elevation map of Central Asia with the location of weather stations in which March temperature records were broken - T<sub>max</sub> records in red, T<sub>min</sub> records in blue, both in purple. The study region is shown in dark red.

In mid-March 2025, a region of central Asia experienced extreme temperature anomalies of more than 10 °C in 5-daily maximum and minimum temperatures (Fig. 1.1). The region has geographically diverse climatology driven by the complex orography in the east, falling to arid lowlands to the north and west (Fig. 1.2). In order to account for this and minimise the influence of altitude, the study region contains only the low-lying regions along the borders of Uzbekistan, Turkmenistan, Kazakhstan, and low-lying parts of Tajikistan and Kyrgyzstan, and is bounded by 47 °N and 60 °E.

This region has a strong seasonal cycle in both daily maximum and minimum temperatures (Fig. 1.3), with low variability and a stark difference between winter and summer temperatures of approximately 40 °C. As a result, we consider changes in temperature extremes in March only, to ensure that the trends pertain to this period of early heat rather than the more expected late spring and summertime extremes. Even this choice likely results in studying changes in late March extremes, given the rapid increase in temperatures through March itself.

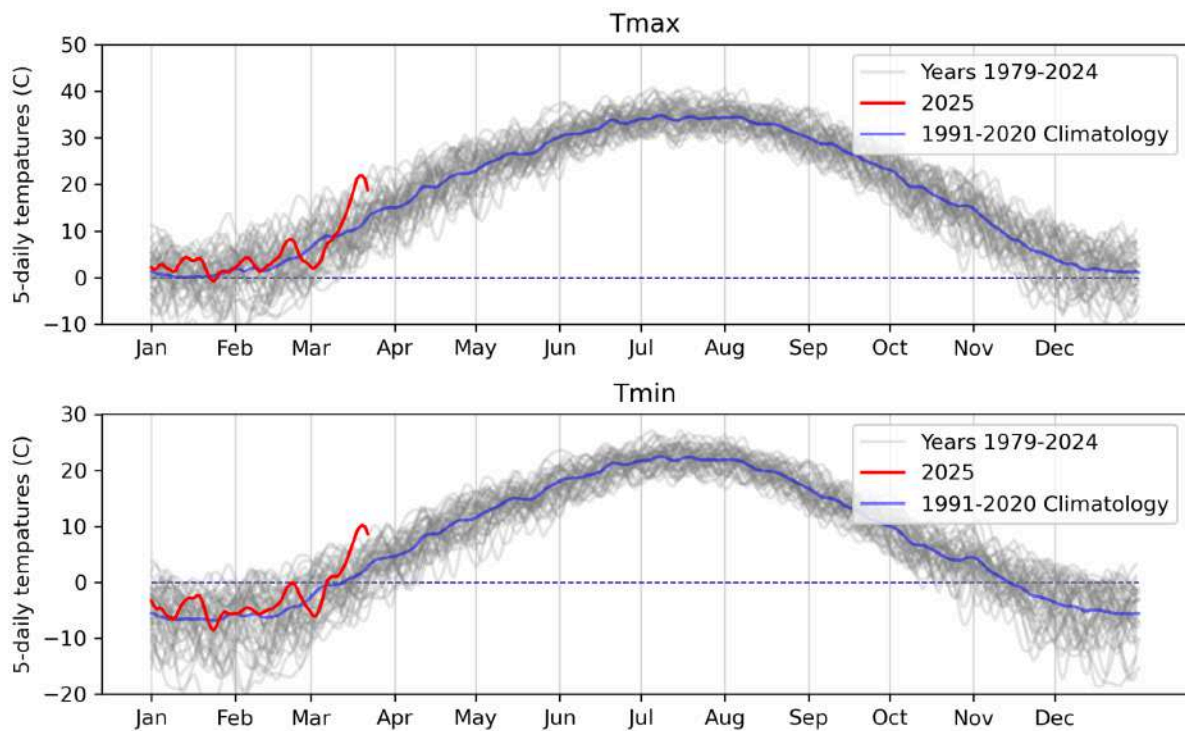


Figure 1.3: Seasonal cycles of 5-daily maximum (top) and minimum (bottom) over the study region, for all years in the dataset (MSWX). The 1991-2020 climatology is shown in blue and the 2025 temperatures in red.

In this study, we analyse changes in the extreme early heat using two metrics:

1. Tx5day - March 5-day maximum of daily maximum temperatures averaged over the study region (Fig. 1.1)
2. Tn5day - March 5-day maximum of daily minimum temperatures averaged over the study region (Fig. 1.1)

We study the influence of anthropogenic climate change by comparing the likelihood and intensity of similar early heat extremes at present with those in a 1.3 °C cooler climate. We also extend this analysis into the future by assessing the influence of a further 1.3 °C of global warming from present. This is in line with the latest Emissions Gap Report from the United Nations Environment Programme, which shows that the world is on track for at least 2.6 °C temperature rise given currently implemented policies ([UNEP, 2024](#)).

## 2 Data and methods

### 2.1 Observational data

We first use observational and reanalysis data to estimate the return period of a similar event in the present day and to assess the historical trends with increasing GMST. The datasets used are as follows:

1. **ERA5** - The European Centre for Medium-Range Weather Forecasts's 5th generation reanalysis product, ERA5, is a gridded dataset that combines historical observations into global estimates using advanced modelling and data assimilation systems ([Hersbach et al., 2020](#)). We use daily maximum and minimum temperature data from this product at a resolution of  $0.5^{\circ} \times 0.5^{\circ}$ , from the years 1950 to 28th February 2025.
2. **MSWX** - The Multi-Source Weather dataset ([Beck et al., 2022](#)), which combines various observational and reanalysis-based data for reliable bias-corrected weather variable estimates, at 3-hourly intervals from 1979 to near real-time (used up to 24th March 2025), and at  $0.1^{\circ}$  spatial resolution globally.
3. **CPC** - We use the daily maximum and daily minimum temperatures from the gridded product from NOAA PSL, Boulder, Colorado, USA known as the CPC Global Unified Daily Gridded data, available at  $0.5^{\circ} \times 0.5^{\circ}$  resolution, for the period 1979 - 24th March 2025. Data are available from [NOAA](#).
4. **GHCN-D** - We use local stations from the Global Historical Climatology Network daily (GHCNd), an integrated database of daily climate summaries from land surface stations across the globe. We use time series of daily maximum and minimum temperatures from station IDs: KG000038613, KZ000035849, KZ000038198, TI000038933, TX000038974, UZM00038611, UZM00038618, where there are at least 45 years of data and where the Tx5day and Tn5day time series have a value in at least 90% of years. Missing values in the extremes time series are linearly interpolated.

Finally, as a measure of anthropogenic climate change we use the (low-pass filtered) global mean surface temperature (GMST), where GMST is taken from the National Aeronautics and Space Administration (NASA) Goddard Institute for Space Science (GISS) surface temperature analysis (GISTEMP, [Hansen et al., 2010](#) and [Lenssen et al., 2019](#)).

### 2.2 Model and experiment descriptions

We use 2 multi-model ensembles from climate modelling experiments using very different framings ([Philip et al., 2020](#)): Sea Surface temperature (SST) driven global circulation high resolution models, coupled global circulation models and regional climate models.

1. CMIP6. This consists of simulations from 18 participating models with varying resolutions. For more details on CMIP6, please see [Eyring et al., \(2016\)](#). For all simulations, the period 1850 to 2015 is based on historical simulations, while the SSP5-8.5 scenario is used for the remainder of the 21st century.

2. HighResMIP SST-forced model ensemble ([Haarsma et al. 2016](#)), the simulations for which span from 1950 to 2050. The SST and sea ice forcings for the period 1950-2014 are obtained from the 0.25° x 0.25° Hadley Centre Global Sea Ice and Sea Surface Temperature dataset that have undergone area-weighted regridding to match the climate model resolution (see Table B). For the ‘future’ time period (2015-2050), SST/sea-ice data are derived from RCP8.5 (CMIP5) data, and combined with greenhouse gas forcings from SSP5-8.5 (CMIP6) simulations (see Section 3.3 of Haarsma et al. 2016 for further details).

### **2.3 Statistical methods**

Methods for observational and model analysis and for model evaluation and synthesis are used according to the World Weather Attribution Protocol, described in [Philip et al., \(2020\)](#), with supporting details found in [van Oldenborgh et al., \(2021\)](#), [Ciavarella et al., \(2021\)](#) and [here](#). The key steps, presented in sections 3-6, are: (3) trend estimation from observations; (4) model validation; (5) multi-method multi-model attribution; and (6) synthesis of the attribution statement.

In this report we analyse time series of the maximum March 5-day daily maximum and minimum temperatures in a region over Central Asia. For each time series we calculate the return period and intensity of the event under study for the 2025 GMST and for 1.3 °C cooler GMST: this allows us to compare the climate of now and of the preindustrial past (1850-1900, based on the [Global Warming Index](#)), by calculating the probability ratio (PR; the factor-change in the event's probability) and change in intensity of the event.

A nonstationary generalised extreme value (GEV) distribution is used to model both indices. For temperatures, the distribution is assumed to shift linearly with the covariates, while the variance remains constant. The parameters of the statistical model are estimated using maximum likelihood.

### 3 Observational analysis: return period and trend

#### 3.1 Analysis of point station data and gridded data

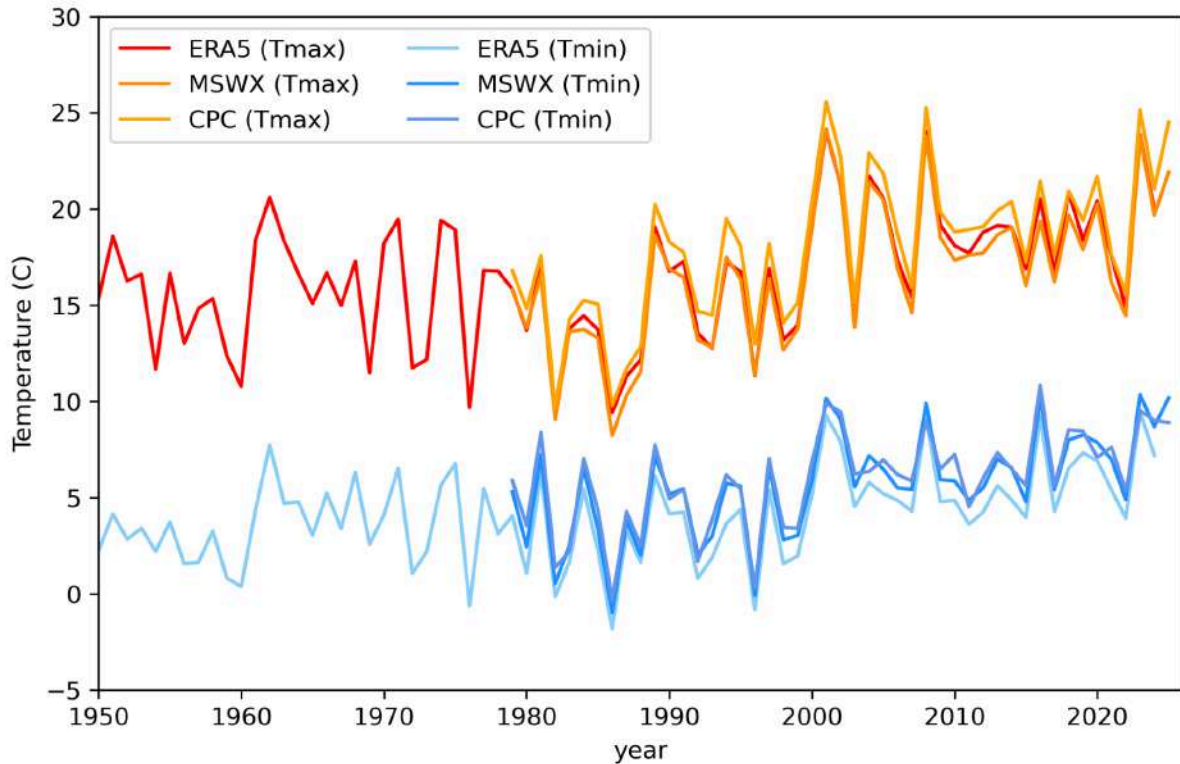


Figure 3.1: Time series of Tx5day and Tn5day in all reanalysis and observational datasets used in this study.

Averaged over the whole study region, the 2025 event(s) are relatively common in the present climate, with return periods of approximately 3 years (tables 3.1 & 3.2). Such an event would have been extremely rare in the preindustrial climate. The current warming level of 1.3 °C resulted in a huge increase in both metrics. For Tx5day, we find increases by a factor of at least 14 in PR, with best estimates ranging from 150 to tens of thousands, and 6-11 °C in intensity. The increase is most pronounced during the period common to all datasets, from 1979 onwards, shown by studying changes in ERA5 across the common period of 1979-present, which results in a probability ratio increase by a further factor of 50 and increase in intensity of approximately a further 5 °C relative to using the entire time series (Fig. 3.1, Table 3.1).

Similarly, for Tn5day, we find increases of a factor of at least 12 in PR, with best estimates of infinity in datasets containing the event, and 4-8 °C in intensity for Tn5day (Table 3.2). The rapid increase in the strength of the trend from 1979 onwards is also observed in this metric (Fig. 3.1, Table 3.2). The best estimates suggest that in a preindustrial climate, such events would have occurred once only every few hundred years, if at all. Perhaps more notably, both metrics are becoming hotter far more rapidly than global mean surface temperature, indicating a potential role for both thermodynamics and dynamical climate influences.

To explore the extremely strong trends in March 5-day extremes further, we also check changes in individual local weather stations from around the region (Tables A.1 & A.2, Fig. A.1), and in gridded products in 1-day extremes in March (Table A.3) and annual 5-day maxima (Table A.4).

Local weather stations show similar trends to gridded products to Tx5day. 6 out of the 7 stations show trends that are statistically significant at the 95% confidence level, with best estimates (including the non-significant estimate) ranging from a 3-33-fold increase. Crucially, these stations also show comparably large increases in magnitude above GMST rise, from 2.5-8 °C. For Tn5day, the changes in local stations are much weaker. Only 1 out of 5 stations show statistical significance, with a 26-fold increase in likelihood and in 3.5 °C intensity, while others give a factor of 1.1-2 in probability and 0.5-1.5 C intensity. This may be related in part to the sparser data availability of daily minimum temperatures from the same stations, and also may indicate that the two metrics are behaving fundamentally differently with respect to climate change at the local scale. Further analysis is required to elucidate this connection in the local conditions.

Considering the gridded products again, the trends in both metrics are comparatively extreme when considering the 1-day March maxima, suggesting that the event definition isn't sensitive to the time period used. The more striking result arises from analysis of the annual 5-day maxima in both metrics, which generally occur from June-August due to the strength of the seasonal cycles. In these metrics compared to March only, we observe very similar probability ratios approaching infinity, but changes in intensity that are large but much closer to global surface temperature rise of 1.7-3.2 °C in Tx5day and 1.5-2.8 °C in Tn5day (Table A.4). This suggests that changes in the early season heat are occurring more rapidly than the overall regional trend in extreme heat.

Dataset	Event		GMST trend	
	Magnitude (°C)	Return period (95% C.I.)	Probability Ratio	Change in magnitude (°C)
MSWX	21.92	2.41 (1.41 - 4.99)	<b>1992.02</b> <b>(25.70 - inf)</b>	<b>10.43</b> <b>(6.97 - 15.17)</b>
CPC	24.51	3.30 (1.70 - 8.20)	<b>33400</b> <b>(34.77 - inf)</b>	<b>10.71</b> <b>(6.91 - 15.50)</b>
ERA5	20.94	3	<b>152.83</b> <b>(13.70 - inf)</b>	<b>5.85</b> <b>(3.63 - 8.27)</b>
ERA5 (1979 onwards)	21.87	3	<b>72177.29</b> <b>(49.80 - inf)</b>	<b>10.50</b> <b>(7.00 - 15.32)</b>

Table 3.1: Estimated return periods of Tx5day events over the Central Asia region in the two reanalysis datasets (MSWX and CPC) with coverage of the event, plus ERA5 which is used to study trends only, as well as probability ratio and change in magnitude with increasing GMST. Statistically significant trends are highlighted in **bold font**.

Dataset	Event		GMST trend	
	Magnitude (°C)	Return period (95% C.I.)	Probability Ratio	Change in magnitude (°C)
MSWX	10.18	2.90 (1.59 - 7.77)	<b>Inf</b> <b>(629.32 - inf)</b>	<b>7.94</b> <b>(4.97 - 11.56)</b>
CPC	8.90	1.87 (1.21 - 3.65)	<b>Inf</b> <b>(185.95 - inf)</b>	<b>6.73</b> <b>(3.57 - 10.56)</b>
ERA5	7.24	3	<b>90.14</b> <b>(12.05 - inf)</b>	<b>4.03</b> <b>(2.57 - 5.76)</b>
ERA5 (1979 onwards)	8.11	3	<b>Inf</b> <b>(83.63 - inf)</b>	<b>7.73</b> <b>(4.90 - 11.35)</b>

Table 3.2: Estimated return periods of Tn5day events over the Central Asia region in the two reanalysis datasets (MSWX and CPC) with coverage of the event, plus ERA5 which is used to study trends only, as well as probability ratio and change in magnitude with increasing GMST. Statistically significant trends are highlighted in **bold font**.

### 3.2 Rapidly increasing intensity of early heatwaves

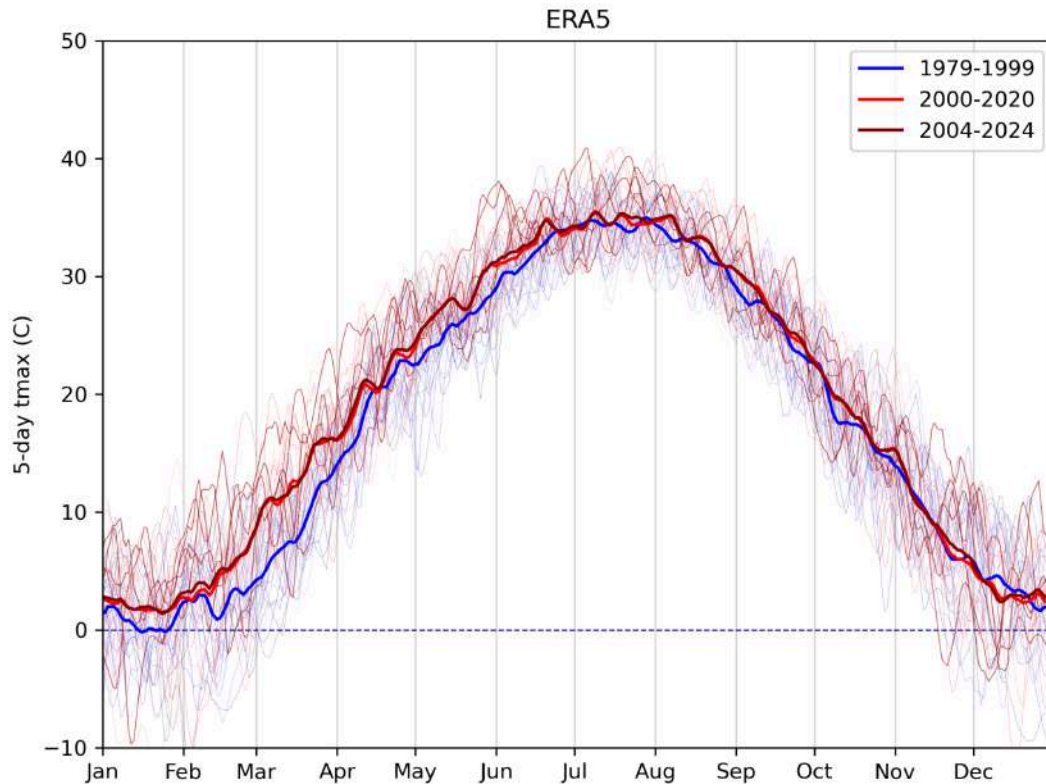


Figure 3.2: Seasonal cycles of 5-day averaged daily maximum temperatures in ERA5. The blue line shows the 1979-1999 average seasonal cycle, and the red (dark red) line shows the 2000-2020

(2004-2024) average seasonal cycle. Individual years are shown as thinner lines with colour from blue to red indicating the year from 1979-2024 (the years 2020-2024 are bold).

In order to study the changes in early season extremes in more detail, we investigate the changes in the seasonal cycles. Figure 3.2 shows the rolling 5-day mean of daily maximum temperatures in every year from 1979-2024, alongside the 1979-1999 mean and 2000-2020 means. This shows a striking change in the shape of the seasonal cycle over just these two periods, with little change across most of the year but a significant offset of approximately 5 C in the period around March. This is observed in all gridded data products (Fig. A.2), and is particularly stark in March compared to other months (Fig. A.3). Furthermore, the same is observed across all individual weather stations in spite of local climatological variations (Fig. 3.3). All figures are shown for daily maximum temperatures but a similar phenomenon is also observed in daily minimum temperatures. This phenomenon requires further exploration that is beyond the scope of a rapid study. However, given that climate models are used to analyse changes in similar extremes, we also check whether this phenomenon is captured. Figure A.4 & A.5 show the seasonal cycles in CMIP6 models from preindustrial conditions (1850-1880) compared to the end of the 21st century (2070-2100), with the mean difference removed. No model represents the more rapid increase in heat in spring compared to the rest of the year. This is also the case for HighResMIP models (Fig A.5). As a result, while we still use these models for the attribution analysis, the changes are consistently underestimated.

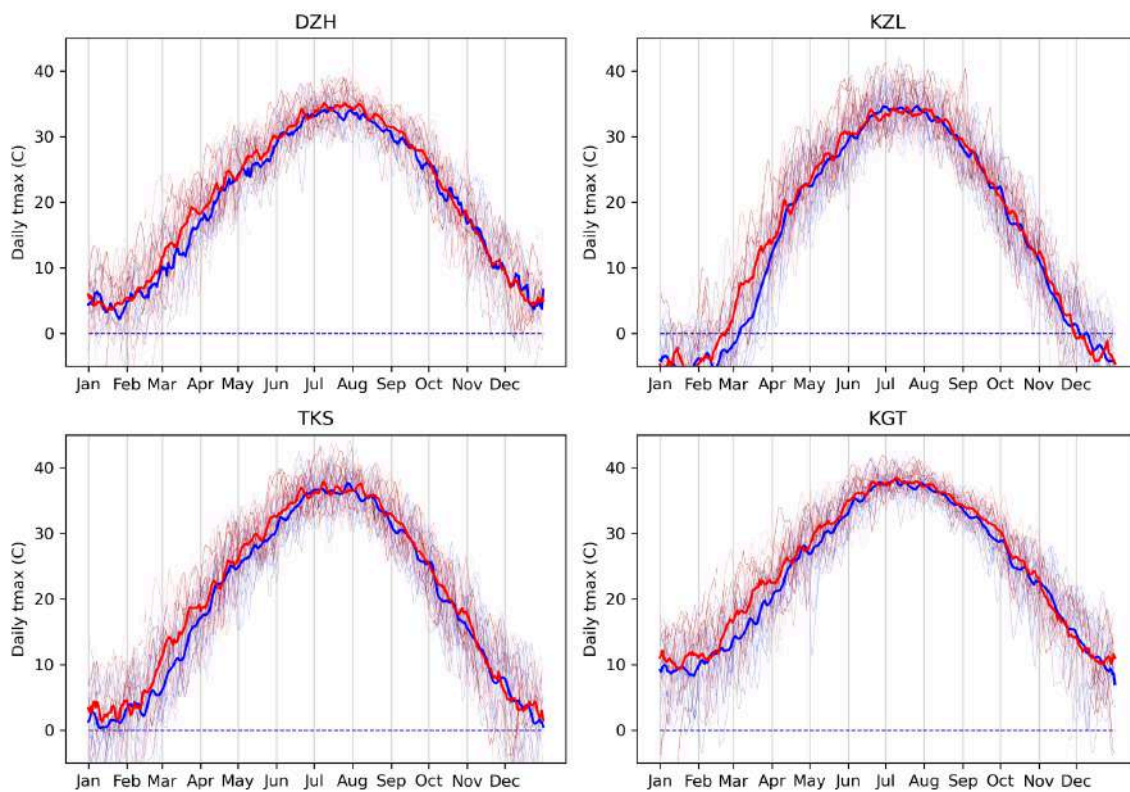


Figure 3.3: Seasonal cycles of 5-day averaged daily maximum temperatures in four local weather stations. The blue line shows the 1979-1999 average seasonal cycle, and the red line shows the 2000-2020 average seasonal cycle. Individual years are shown as thinner lines with colour from blue to red indicating the year from 1979-2024 (the years 2020-2024 are bold).

## 4 Model evaluation

In the subsections below we show the results of the model evaluation. The climate models are evaluated against the observations in their ability to capture:

1. Seasonal cycles: For this, we qualitatively compare the seasonal cycles based on model outputs against observations-based cycles. We discard the models that exhibit ill-defined peaks in their seasonal cycles. We also discard the model if the rainy season onset/termination varies significantly from the observations.
2. Spatial patterns: Models that do not match the observations in terms of the large-scale precipitation patterns are excluded.
3. Parameters of the fitted statistical models. We discard the model if the model and observation parameters ranges do not overlap.

The models are labelled as 'good', 'reasonable', or 'bad' based on their performances in terms of the three criteria discussed above. A model is given an overall rating of 'good' if it is rated 'good' for all three characteristics. If there is at least one 'reasonable', then its overall rating will be 'reasonable' and 'bad' if there is at least one 'bad'. For each framing or model setup we also use models that only just pass the evaluation tests if we only have five models or less for that framing that perform well.

For Tx5day, 5 out of 14 CMIP6 models and 6 out of 12 HighResMIP models are ranked as 'good' and therefore only these are used (Table 4.1). For Tn5day, 8 out of 11 CMIP6 models and 2 out of 12 HighResMIP models are ranked as 'good', therefore only these are used for CMIP6, and all models (ranked as 'reasonable') are used from HighResMIP (Table 4.2). The model evaluation figures are shown in the appendix (Figs. A.6-A.13)

### 4.1 Tx5day

Model / Observations	Seasonal cycle	Spatial pattern	Sigma	Shape parameter	Summary	Used in analysis? (Y/N)
MSWX			2.84 (2.19 ... 3.30)	-0.19 (-0.45 ... 0.047)		
CPC			2.95 (2.27 ... 3.47)	-0.21 (-0.45 ... 0.0068)		
ERA5			3.08 (2.63 ... 3.54)	-0.32 (-0.52 ... -0.18)		
<b>CMIP6</b>						
ACCESS-CM2 (1)	reasonable	good	3.26 (2.23 ... 4.37)	-0.20 (-0.63 ... 0.18)	reasonable	N
ACCESS-ESM1-5 (1)	good	good	3.14 (2.24 ... 3.92)	-0.46 (-0.82 ... -0.14)	good	Y
CMCC-ESM2 (1)	good	good	3.60 (2.69 ... 4.30)	-0.15 (-0.41 ... 0.027)	reasonable	N
CNRM-CM6-1 (1)	good	good	3.29 (2.49 ... 3.91)	-0.092 (-0.39 ... 0.14)	good	Y
EC-Earth3 (1)	good	good	3.06 (2.44 ... 3.68)	-0.24 (-0.74 ... -0.053)	good	Y

EC-Earth3-Veg (1)	good	good	2.86 (2.17 ... 3.52)	-0.23 (-0.64 ... 0.033)	good	Y
FGOALS-g3 (1)	reasonable	reasonable	2.42 (1.52 ... 2.98)	-0.29 (-0.68 ... 0.36)	reasonable	N
INM-CM4-8 (1)	reasonable	good	3.24 (2.43 ... 4.00)	-0.45 (-0.85 ... -0.28)	reasonable	N
INM-CM5-0 (1)	reasonable	good	2.86 (2.21 ... 3.38)	-0.24 (-0.71 ... -0.12)	reasonable	N
MIROC6 (1)	good	good	2.48 (1.90 ... 2.90)	-0.25 (-0.52 ... 0.049)	reasonable	N
MPI-ESM1-2-HR (1)	good	good	3.55 (2.63 ... 4.36)	-0.35 (-0.66 ... -0.069)	reasonable	N
MPI-ESM1-2-LR (1)	reasonable	good	2.56 (1.90 ... 3.14)	-0.32 (-0.64 ... -0.10)	reasonable	N
MRI-ESM2-0 (1)	good	good	3.15 (2.40 ... 3.90)	-0.23 (-0.71 ... 0.0046)	good	Y
NorESM2-LM (1)	reasonable	good	3.13 (2.17 ... 3.78)	-0.44 (-0.76 ... -0.14)	reasonable	N
<b>HighResMIP</b>						
CNRM-CM6-1-HR (1)	good	good	3.32 (2.79 ... 3.77)	-0.23 (-0.51 ... -0.11)	good	Y
EC-Earth3P-HR (1)	good	good	2.96 (2.41 ... 3.45)	-0.33 (-0.61 ... -0.22)	good	Y
FGOALS-f3-L (1)	good	good	3.24 (1.76 ... 4.24)	-0.34 (-0.79 ... 0.37)	good	Y
HadGEM3-GC31-HM (1)	good	good	3.26 (2.64 ... 3.79)	-0.24 (-0.44 ... -0.12)	good	Y
HadGEM3-GC31-LM (1)	good	good	4.00 (2.39 ... 4.98)	-0.37 (-0.71 ... 0.026)	reasonable	N
HadGEM3-GC31-MM (1)	good	good	3.52 (2.00 ... 4.26)	-0.44 (-0.77 ... 0.32)	good	Y
HiRAM-SIT-HR (1)	good	good	2.95 (2.08 ... 3.64)	-0.36 (-0.66 ... -0.11)	good	Y
HiRAM-SIT-LR (1)	good	good	2.09 (1.40 ... 2.56)	-0.12 (-0.52 ... 0.16)	reasonable	N
MPI-ESM1-2-HR (1)	reasonable	good	3.23 (2.02 ... 3.96)	-0.35 (-0.65 ... -0.069)	reasonable	N
MPI-ESM1-2-XR (1)	reasonable	good	3.12 (1.91 ... 3.85)	-0.37 (-0.71 ... 0.11)	reasonable	N
NICAM16-7S (1)	reasonable	good	2.30 (1.08 ... 3.02)	-0.20 (-0.48 ... 0.48)	reasonable	N
NICAM16-8S (1)	reasonable	good	2.25 (1.36 ... 2.84)	-0.33 (-0.68 ... 0.17)	good	N

*Table 4.1 Evaluation results of the climate models considered for attribution analysis of Tx5day. For each model, the threshold for a 1-in-3-year event is shown, along with the best estimates of the Sigma and Shape parameters are shown, along with 95% confidence intervals. Furthermore evaluation of the seasonal cycle and spatial pattern are shown.*

## 4.2 Tn5day

Model / Observations	Seasonal cycle	Spatial pattern	Sigma	Shape parameter	Summary	Used in analysis? (Y/N)
----------------------	----------------	-----------------	-------	-----------------	---------	-------------------------

MSWX			2.12 (1.50 ... 2.54)	-0.28 (-0.51 ... -0.054)		
CPC			2.10 (1.52 ... 2.54)	-0.32 (-0.57 ... -0.066)		
ERA5			2.21 (1.75 ... 2.58)	-0.32 (-0.45 ... -0.15)		
<b>CMIP6</b>						
CMCC-ESM2 (1)	good	good	2.15 (1.51 ... 2.67)	-0.20 (-0.48 ... 0.070)	good	Y
CNRM-CM6-1 (1)	good	good	2.50 (1.71 ... 3.04)	-0.18 (-0.54 ... 0.077)	good	Y
EC-Earth3-Veg (1)	good	good	1.97 (1.46 ... 2.34)	-0.21 (-0.49 ... 0.12)	good	Y
FGOALS-g3 (1)	reasonable	reasonable	2.11 (1.52 ... 2.54)	-0.47 (-0.81 ... 0.065)	reasonable	N
INM-CM4-8 (1)	good	good	1.73 (1.03 ... 2.13)	-0.14 (-0.33 ... 0.28)	good	Y
INM-CM5-0 (1)	good	good	2.14 (1.63 ... 2.54)	-0.20 (-0.94 ... -0.084)	good	Y
MIROC6 (1)	good	good	1.82 (1.44 ... 2.16)	-0.36 (-0.69 ... -0.14)	good	Y
MPI-ESM1-2-HR (1)	good	good	2.43 (1.79 ... 2.98)	-0.27 (-0.67 ... 0.027)	good	Y
MPI-ESM1-2-LR (1)	good	reasonable	1.92 (1.53 ... 2.30)	-0.36 (-0.74 ... -0.16)	reasonable	N
NorESM2-LM (1)	reasonable	reasonable	2.21 (1.53 ... 2.81)	-0.29 (-0.69 ... -0.043)	reasonable	N
NorESM2-MM (1)	good	good	2.12 (1.18 ... 2.64)	-0.28 (-0.59 ... 0.21)	good	Y
<b>HighResMIP</b>						
CNRM-CM6-1-HR (1)	good	good	2.62 (2.22 ... 3.02)	-0.26 (-0.59 ... -0.16)	reasonable	Y
EC-Earth3P-HR (1)	good	good	2.37 (1.83 ... 2.83)	-0.51 (-0.69 ... -0.35)	good	Y
FGOALS-f3-L (1)	good	good	1.59 (1.05 ... 2.23)	-0.19 (-0.72 ... 0.042)	good	Y
HadGEM3-GC31-HM (1)	reasonable	good	2.13 (1.79 ... 2.45)	-0.25 (-0.61 ... -0.12)	reasonable	Y
HadGEM3-GC31-LM (1)	reasonable	good	2.25 (1.75 ... 2.67)	-0.27 (-0.57 ... -0.12)	reasonable	Y
HadGEM3-GC31-MM (1)	reasonable	good	2.44 (2.02 ... 2.95)	-0.42 (-0.70 ... -0.26)	reasonable	Y
HiRAM-SIT-HR (1)	reasonable	good	2.27 (1.31 ... 2.85)	-0.19 (-0.51 ... 0.27)	reasonable	Y
HiRAM-SIT-LR (1)	reasonable	good	1.70 (0.992 ... 2.29)	0.014 (-0.37 ... 0.61)	reasonable	Y
MPI-ESM1-2-HR (1)	reasonable	good	2.12 (1.62 ... 2.48)	-0.17 (-0.31 ... -0.033)	reasonable	Y
MPI-ESM1-2-XR (1)	reasonable	good	2.30 (1.89 ... 2.66)	-0.46 (-0.65 ... -0.29)	reasonable	Y
NICAM16-7S (1)	reasonable	good	1.66 (0.991 ... 2.14)	-0.064 (-0.35 ... 0.38)	reasonable	Y
NICAM16-8S (1)	reasonable	good	1.67 (1.07 ... 2.26)	-0.18 (-0.64 ... 0.35)	reasonable	Y

Table 4.2: Evaluation results of the climate models considered for attribution analysis of Tn5day. For each model, the threshold for a 1-in-3-year event is shown, along with the best estimates of the Sigma and Shape parameters are shown, along with 95% confidence intervals. Furthermore evaluation of the seasonal cycle and spatial pattern are shown.

## 5 Multi-method multi-model attribution

This section shows Probability Ratios and change in intensity  $\Delta I$  for models that passed model evaluation and also includes the values calculated from the fits with observations.

### 5.1 Tx5day

Model / Observations	Threshold for return period 3 yr	Preindustrial - Present (1.3 °C)		Present - Future (2.6 °C)	
		Probability ratio PR [-]	Change in intensity $\Delta I$ [°C]	Probability ratio PR [-]	Change in intensity $\Delta I$ [°C]
MSWX	21.92 °C	2.0e+3 (26 ... 9.3e+8)	10 (7.0 ... 15)		
CPC	24.51 °C	3.3e+4 (35 ... 3.0e+13)	11 (6.9 ... 16)		
ERA5	20.94 °C	1.5e+2 (14 ... 2.1e+5)	5.8 (3.6 ... 8.3)		
ACCESS-ES M1-5 (1)	16 °C	1.5 (0.81 ... 3.5)	1.1 (-0.66 ... 2.8)	1.7 (1.4 ... 2.0)	1.8 (1.1 ... 2.5)
CNRM-CM6-1 (1)	19 °C	2.1 (1.1 ... 4.5)	2.4 (0.40 ... 4.0)	1.6 (1.3 ... 1.9)	2.0 (0.89 ... 2.8)
EC-Earth3 (1)	19 °C	1.6 (0.96 ... 2.9)	1.5 (-0.13 ... 3.0)	1.6 (1.4 ... 1.9)	2.0 (1.3 ... 2.7)
EC-Earth3-Ve g (1)	20 °C	1.7 (1.1 ... 2.8)	1.4 (0.15 ... 2.6)	1.6 (1.3 ... 1.9)	1.6 (0.89 ... 2.3)
MRI-ESM2-0 (1)	18 °C	1.2 (0.62 ... 3.0)	0.47 (-1.7 ... 2.4)	1.3 (1.0 ... 1.6)	0.94 (0.13 ... 1.7)
CNRM-CM6-1 -HR (1)	22 °C	4.5 (1.4 ... $\infty$ )	3.7 (0.99 ... 7.6)	1.7 (1.3 ... 2.2)	2.1 (0.86 ... 3.5)
EC-Earth3P-H R (1)	22 °C	41 (3.6 ... $\infty$ )	4.9 (2.3 ... 7.5)	2.0 (1.5 ... 2.5)	2.6 (1.3 ... 4.1)
FGOALS-f3-L (1)	17 °C	0.81 (0.41 ... $\infty$ )	-0.68 (-3.8 ... 3.4)		
HadGEM3-G C31-HM (1)	21 °C	9.9 (2.0 ... $\infty$ )	4.9 (1.9 ... 8.2)	2.3 (1.9 ... 2.8)	3.9 (2.6 ... 5.3)
HadGEM3-G C31-MM (1)	21 °C	20 (2.4 ... $\infty$ )	5.3 (2.1 ... 8.8)		
HiRAM-SIT-H R (1)	23 °C	8.0 (1.4 ... $\infty$ )	3.4 (0.80 ... 6.3)		

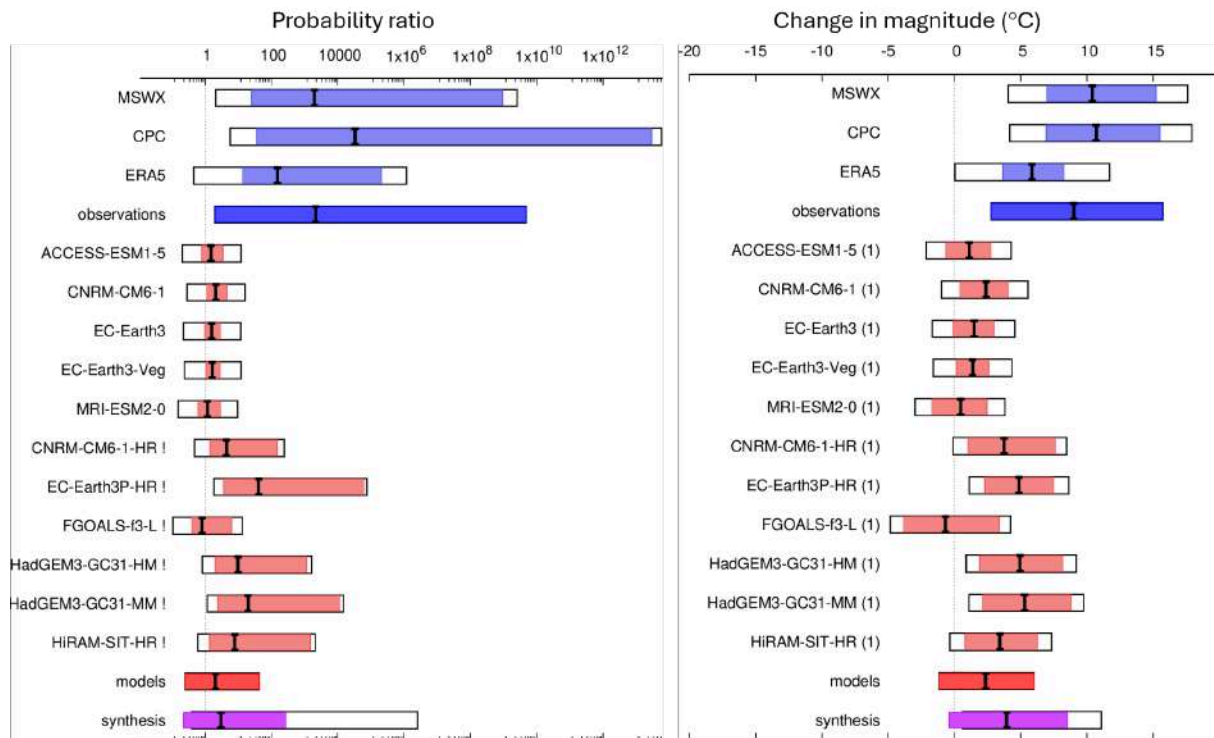
Table 5.1: Event magnitude, probability ratio and change in intensity for 3-year return period for Tx5day for observational datasets and each model that passed the evaluation tests. (a) from pre-industrial climate to the present and (b) from the present to 2.6 °C above pre-industrial climate.

## 5.2 Tn5day

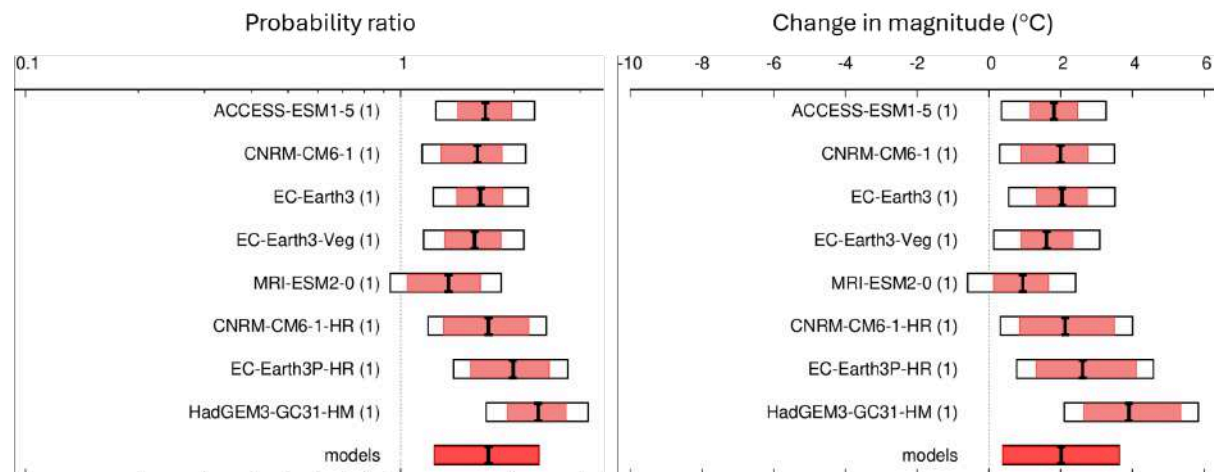
Model / Observations	Threshold for return period 3 yr	Preindustrial - Present (1.3 °C)		Present - Future (2.6 °C)	
		Probability ratio PR [-]	Change in intensity $\Delta I$ [°C]	Probability ratio PR [-]	Change in intensity $\Delta I$ [°C]
CPC	8.9 °C	$\infty$ (1.9e+2 ... $\infty$ )	6.7 (3.6 ... 11)		
ERA5	7.24 °C	90 (12 ... $\infty$ )	4.0 (2.6 ... 5.8)		
CMCC-ESM2 (1)	6.3 °C	2.0 (1.2 ... 3.7)	1.5 (0.51 ... 2.6)	2.0 (1.7 ... 2.3)	2.3 (1.6 ... 2.9)
CNRM-CM6-1 (1)	5.7 °C	2.3 (1.2 ... 5.3)	1.8 (0.39 ... 3.0)	1.7 (1.4 ... 2.0)	1.7 (0.97 ... 2.3)
EC-Earth3-Veg (1)	5.9 °C	3.2 (1.8 ... 7.2)	1.9 (1.1 ... 2.8)	1.9 (1.7 ... 2.2)	1.9 (1.4 ... 2.5)
INM-CM4-8 (1)	4.9 °C	1.4 (0.82 ... 3.1)	0.65 (-0.40 ... 1.8)	1.6 (1.2 ... 2.0)	1.0 (0.45 ... 1.7)
INM-CM5-0 (1)	5.8 °C	1.5 (0.59 ... 3.9)	0.84 (-1.3 ... 2.3)	1.9 (1.6 ... 2.3)	1.9 (1.2 ... 2.7)
MIROC6 (1)	9.2 °C	15 (3.1 ... $\infty$ )	3.0 (1.6 ... 4.3)	2.4 (2.1 ... 2.7)	2.8 (2.0 ... 3.5)
MPI-ESM1-2-HR (1)	9.7 °C	6.3 (2.2 ... 32)	3.0 (1.5 ... 4.5)	2.2 (1.9 ... 2.5)	2.7 (1.9 ... 3.6)
NorESM2-MM (1)	9.7 °C	72 (11 ... $\infty$ )	4.5 (3.2 ... 5.8)	2.4 (2.0 ... 2.7)	3.1 (2.2 ... 4.0)
CNRM-CM6-1-HR (1)	8.5 °C	6.0 (1.4 ... $\infty$ )	3.2 (0.79 ... 6.4)	2.0 (1.6 ... 2.5)	2.4 (1.3 ... 3.5)
EC-Earth3P-HR (1)	8.3 °C	$\infty$ (20 ... $\infty$ )	4.6 (2.3 ... 5.9)	2.3 (1.9 ... 2.6)	2.7 (1.7 ... 3.6)
FGOALS-f3-L (1)	5.7 °C	1.7 (0.61 ... 8.4)	0.87 (-1.2 ... 2.7)		
HadGEM3-GC31-HM (1)	7.5 °C	4.3 (0.98 ... $\infty$ )	2.2 (-0.044 ... 5.0)	2.0 (1.5 ... 2.5)	1.9 (0.95 ... 2.8)
HadGEM3-GC31-LM (1)	7.8 °C	3.9 (0.96 ... $\infty$ )	2.2 (-0.094 ... 4.6)	1.5 (0.97 ... 2.1)	1.1 (-0.065 ... 2.2)
HadGEM3-GC31-MM (1)	7.6 °C	4.3 (0.95 ... $\infty$ )	1.9 (-0.090 ... 3.9)	1.8 (1.3 ... 2.3)	1.5 (0.66 ... 2.5)
HiRAM-SIT-HR (1)	11 °C	10 (1.7 ... $\infty$ )	3.4 (0.99 ... 5.8)		
HiRAM-SIT-LR (1)	11 °C	23 (2.6 ... $\infty$ )	3.8 (1.5 ... 6.1)		
MPI-ESM1-2-HR (1)	10 °C	4.2 (1.4 ... 67)	2.5 (0.58 ... 4.7)	2.0 (1.6 ... 2.5)	1.9 (1.1 ... 2.9)
MPI-ESM1-2-XR (1)	10 °C	2.1 (0.70 ... 1.0e+3)	1.1 (-0.77 ... 2.6)	2.2 (1.8 ... 2.5)	2.7 (1.6 ... 3.4)
NICAM16-7S (1)	7.6 °C	1.8 (0.68 ... 8.9)	1.0 (-0.86 ... 2.8)		
NICAM16-8S (1)	7.0 °C	2.6 (0.76 ... 31)	1.4 (-0.53 ... 3.4)		

Table 5.2: Event magnitude, probability ratio and change in intensity for 3-year return period for Tn5day for observational datasets and each model that passed the evaluation tests. (a) from pre-industrial climate to the present and (b) from the present to 3°C above pre-industrial climate.

## 6 Hazard synthesis



**Figure 6.1:** Synthesised changes for a 3-year  $Tx5day$  event due to GMST. Changes in PR (left) and intensity (right) are shown for a historical period comparing the past  $1.3^{\circ}\text{C}$  cooler climate with the present. If an infinite upper bound has been replaced by a number an exclamation mark has been added to the model name (see Otto et al., 2024).



**Figure 6.2:** Synthesised changes for a 3-year  $Tx5day$  event due to GMST. Changes in PR (left) and intensity (right) are shown for a future period, based on model projections only, comparing the present and a  $2.6^{\circ}\text{C}$  warmed climate (a further  $1.3^{\circ}\text{C}$  above present).

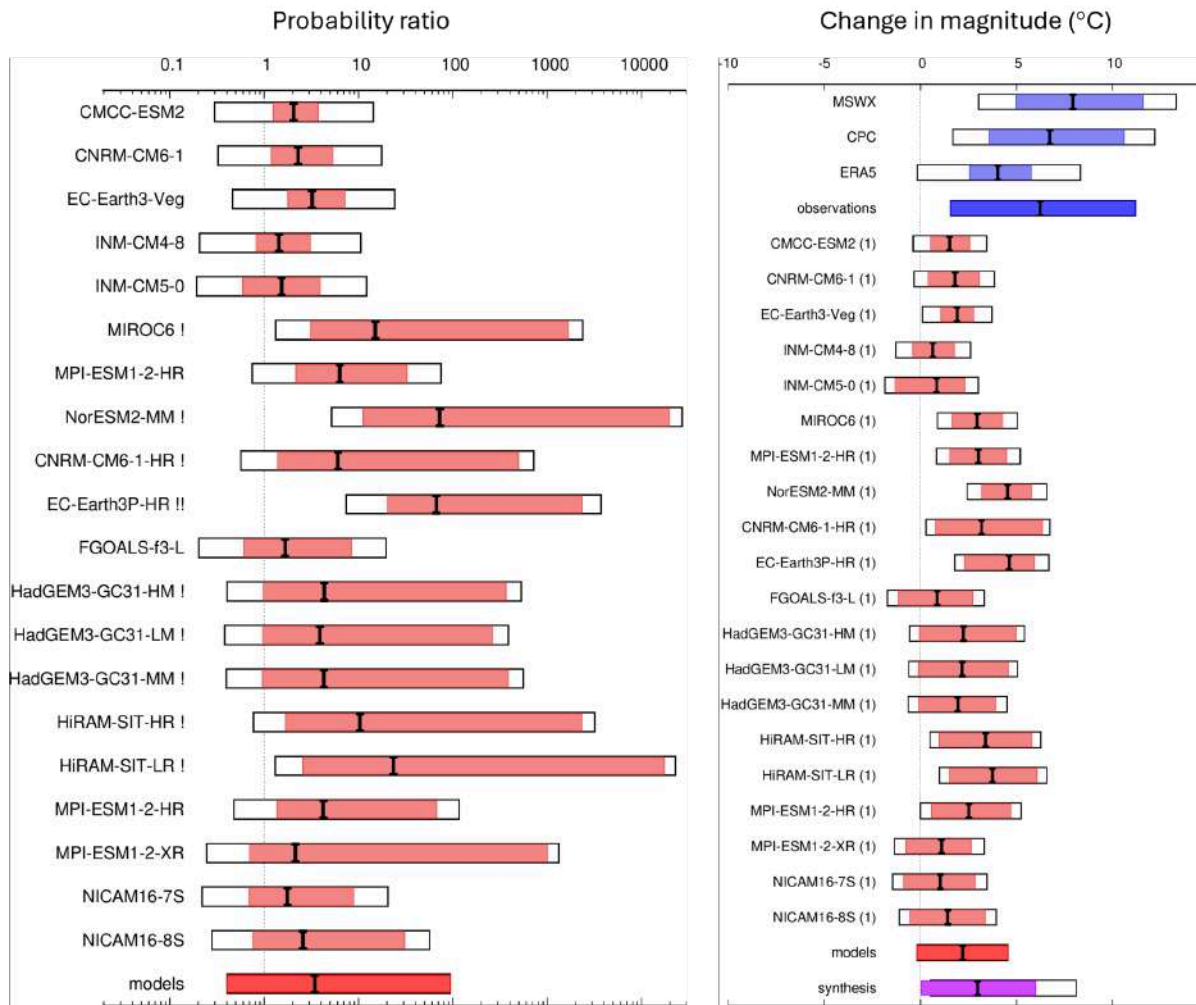


**Figure 6.3:** Synthesised changes for a 3-year  $Tn5day$  event due to GMST. Changes in PR (left) and intensity (right) are shown for a historical period comparing the past  $1.3^{\circ}\text{C}$  cooler climate with the present. If an infinite upper bound has been replaced by a number an exclamation mark has been added to the model name (see Otto et al., 2024).

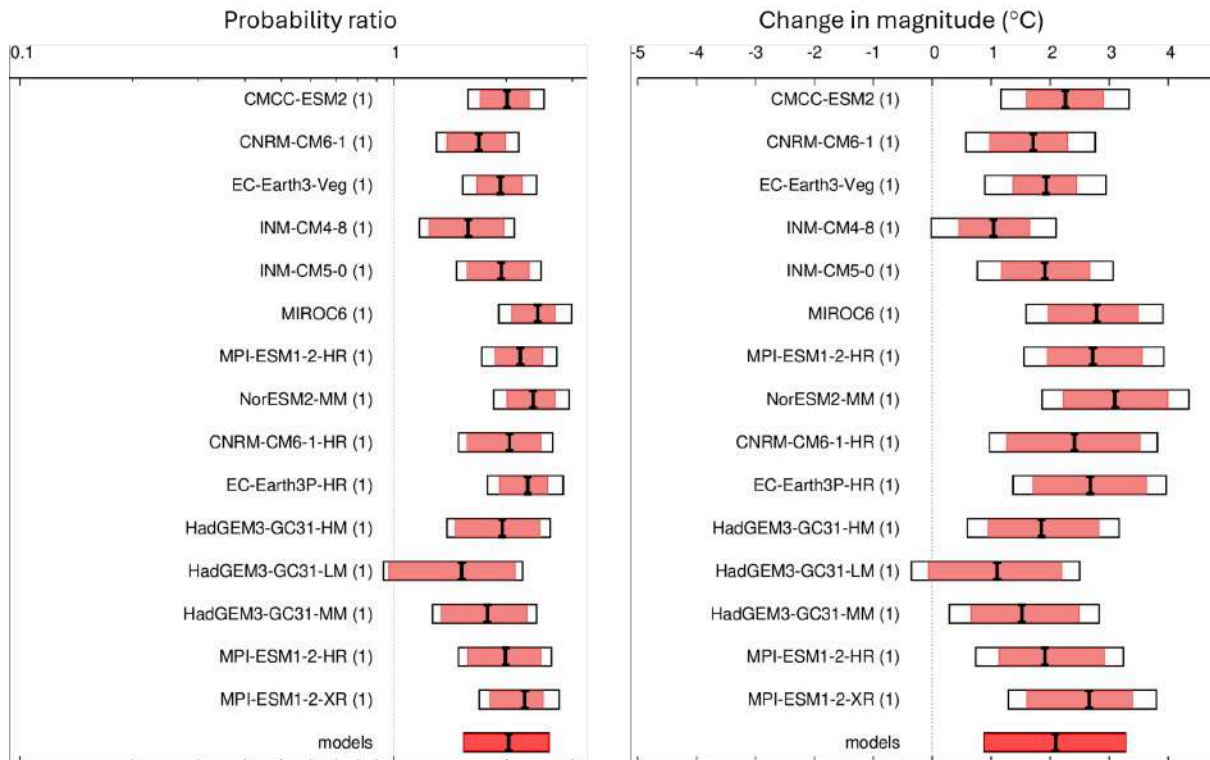


**Figure 6.4:** Synthesised changes for a 3-year  $Tn5day$  event due to GMST. Changes in PR (left) and intensity (right) are shown for a future period, based on model projections only, comparing the present and a 2.6 °C warmed climate (a further 1.3 °C above present).

For the event definitions described above we evaluate the influence of anthropogenic climate change on the events by calculating the probability ratio as well as the change in intensity using observations and climate models. Models which do not pass the evaluation described above are excluded from the analysis. The aim is to synthesise results from models that pass the evaluation along with the observations-based products, to give an overarching attribution statement.

Figures 6.1-6.4 show the changes in probability and intensity for each event definition for the observations (blue) and models (red). Before combining them into a synthesised assessment, first, a representation error is added (in quadrature) to the observations, to account for the difference between observations-based datasets that cannot be explained by natural variability. This is shown in these figures as white boxes around the light blue bars. The dark blue bar shows the average over the observation-based products. Next, a term to account for intermodel spread is added (in quadrature) to the natural variability of the models. This is shown in the figures as white boxes around the light red bars. The dark red bar shows the model average, consisting of a weighted mean using the (uncorrelated) uncertainties due to natural variability plus the term representing intermodel spread (i.e., the inverse square of the white bars).

Observation-based products and models are combined into a single result in two ways. Firstly, we neglect common model uncertainties beyond the intermodel spread that is depicted by the model average, and compute the weighted average of models (dark red bar) and observations (dark blue bar): this is indicated by the magenta bar. As, due to common model uncertainties, model uncertainty can be larger than the intermodel spread, secondly, we also show the more conservative estimate of an unweighted, direct average of observations (dark blue bar) and models (dark red bar) contributing 50% each, indicated by the white box around the magenta bar in the synthesis figures.

Data		Tx5day		Tn5day	
		Probability ratio (95% CI)	Intensity change (°C) (95% CI)	Probability ratio (95% CI)	Intensity change (°C) (95% CI)
<b>Observations</b>	<b>Past - Present</b>	<b>2170</b> (2.04 - 10 <sup>10</sup> )	<b>9.00</b> (2.78 - 15.7)	<b>Infinite</b> (> 90)	<b>6.23</b> (1.56 - 11.2)
<b>Models</b>		2.08 (0.25 - 44.0)	2.36 (-1.18 - 6.02)	3.42 (0.40 - 93.5)	2.20 (-0.17 - 4.54)
<b>Synthesis</b>		3.02 (0.22 - 275.)	3.94 (-0.39 - 8.51)	N/A	2.98 (-0.02 - 6.01)
<b>Models only</b>	<b>Present - Future</b>	<b>1.71</b> (1.23 - 2.33)	<b>2.01</b> (0.40 - 3.63)	<b>2.03</b> (1.54 - 2.60)	<b>2.09</b> (0.88 - 3.28)

Table 6.1: Summary of results for Tx5day and Tn5day, presented in Figs XX: changes due to GMST include past-present changes and present-future changes. Statistically significant changes are highlighted in **bold font**.

Heatwaves around the world are increasing in intensity roughly in line with or just exceeding global mean surface temperature, with the likelihood of exceeding specific temperatures thresholds rising rapidly. This is also true of extreme summer temperatures in western Central Asia. However, here we also find substantial evidence that early heatwaves in this region around March, in both maximum and minimum temperatures, are warming substantially faster than the global and regional averages. This evidence arises from both gridded observational and reanalysis products over the region, and local weather stations. Collectively, this data suggests that as global mean surface temperature has risen by 1.3 °C, early heatwaves like the 2025 event are going from essentially impossible to becoming a common occurrence, roughly every 3 years. Equivalently, 5-day maximum temperatures have increased by about 9 °C (2.8 - 16 °C) and 5-day minimum temperatures by about 6 °C (1.5 - 11 °C).

None of the climate models used are able to represent the change in March temperatures observed in the past ~50 years. However, they pass our other evaluation steps and are therefore used to provide an additional line of evidence that is known to be conservative. Considering models only, we see an increase of approximately 2-2.5 °C (-1 - +6 °C) in the intensity of such events in both metrics, and an increase in likelihood of 2-3.5 (0.25 - 94). None of these estimates are significant at the 95% confidence level. Combining the results from observations and models, we find that Tx5day has become about 3 (0.22 - 275) times as likely and 4 °C (-0.4 - 8.5 °C) more intense, and Tn5day events have become about 3 °C (~0 - 6 °C) more intense. We cannot synthesise the observational and model estimates of likelihood change for Tn5day due to the observations all tending to infinity. The results are not statistically significant, though only a single model gives a decreasing trend for Tx5day and none for Tn5day.

In the future, with a further 1.3 °C of warming from present, models project that such events will become approximately 2 (1.2 - 2.6) times as likely again (occurring twice every 3 years), and another 2 °C (0.4 - 3.6 °C) hotter. This is again in stark contrast to the observational estimates, and therefore form a lower bound on the changes that should be expected in the region given that models do not capture the rapid rise in March temperatures.

Overall, we conclude that early heat events in western Central Asia are increasing in intensity at a

remarkable and dangerous rate, and that global warming of 1.3 °C increased the likelihood by a factor of 3 and magnitude by 4 °C for Tx5day, and a factor of 3 and magnitude by 3 °C for Tn5day. Given current mitigation policies, such events will at least double in likelihood again and become at least 2 °C hotter. Finally, the phenomenon of rapidly increasing intensity of early heatwaves, its relationship to climate change and other drivers, and the inability of climate models to capture this, requires further exploration.

## 7 Vulnerability and exposure

Stretching from the arid lowlands of Turkmenistan and Uzbekistan to the glaciated mountains of Kyrgyzstan and Tajikistan, and into southern Kazakhstan's steppe, this Central Asian region spans varied geographies (see below) and development levels. Human Development Index (HDI) values range from Kazakhstan's "very high" (0.802) to Tajikistan's "medium" (0.679), highlighting disparities in infrastructure and institutional capacity ([UNDP, 2024](#)). This diversity sets the stage for how vulnerabilities unfold across borders, and underscores the importance of context in understanding the risks and impacts of extreme heat in the region.



**Figure 6.5:** The geography of Central Asia. Source: *Green Central Asia* ([2023](#)).

The March 2025 Central Asian heatwave brought record-breaking early-season temperatures, with highs exceeding 30C even at 1000m altitude. The hazard attribution findings indicate a clear fingerprint of human-induced climate change, aligning with long-term projections of significant regional warming - up to 2.75C by 2050 and over 5C by 2090 in parts of Kazakhstan and Tajikistan ([USAID, 2018](#); [World Bank & ADB, 2021](#); [Reyer et al., 2017](#)). These extremes increasingly threaten public health, critical infrastructure, and climate-sensitive sectors such as agriculture and energy ([World Bank & ADB, 2021](#)). It must be noted that research on climate change and vulnerability is very limited in the region ([Vakulchuk et al., 2023](#)). Furthermore, currently there appears to be limited media attention on the ongoing heatwave in the region, making it harder to document vulnerability and exposure with reference to impacts.

Urban areas across the region, including cities like Bishkek and Tashkent, face growing heat exposure due to rapid expansion, limited green cover, and fragmented adaptation efforts, particularly in informal settlements and areas lacking integrated climate planning ([Blondin, 2023](#); [Climate Centre, 2021](#); [Sabyrbekov & Overland, 2023](#)). Under-resourced finance systems and infrastructure already under heat stress further constrain adaptive capacity ([Cohen et al., 2025](#); [World Bank, 2022](#)). Meanwhile, rural and mountainous regions remain highly vulnerable due to fragile infrastructure, low mobility, and high dependence on climate-sensitive livelihoods ([Sabyrbekov & Overland, 2023](#); [GIZ, 2024a](#)). Key at-risk groups include young children, older adults, people with chronic medical

conditions (including cardiovascular, respiratory and kidney disease, diabetes, and mental or cognitive health conditions), outdoor laborers, and rural populations facing infrastructural and institutional constraints ([Broomandi et al., 2024](#); [Sabyrbekov & Overland, 2023](#); [IFRC, 2021](#); [Red Crescent society of Kyrgyzstan, 2019](#); [WFP, 2023b](#); [UNICEF, 2024](#)). The heatwave also underscores structural exposure across energy- and water-intensive economies, where low adaptive capacity magnifies risk.

Exposure to compounding risks is high across the region. High energy and water intensity, along with elevated emissions across countries like Kazakhstan and Turkmenistan, signal structural vulnerability to heat-related infrastructure stress ([Sabyrbekov & Overland, 2023](#)). Glacier retreat in Tajikistan and Kyrgyzstan amplifies local warming and hazard cascades, including landslides and water scarcity ([GIZ, 2021a](#); [Narbayev & Pavlova, 2022](#)). In Turkmenistan and Uzbekistan, baseline aridity intensifies heatwaves through desertification and hydrological stress ([USAID, 2018](#); [Climate Centre, 2021](#)). Urban vulnerability is rising, especially where green space loss intersects with social inequities, as seen in Bishkek ([Blondin, 2023](#)). Although Kazakhstan scores high on the HDI and financial development, the INFORM and World Risk Indexes both highlight moderate-to-high exposure to natural hazards and gaps in coping capacity, particularly at the subnational level where rural infrastructure is more fragile ([UNDRR, 2023a](#); [UNDRR, 2023b](#)).

This analysis explores how vulnerability and exposure patterns shaped the human and sectoral risks of this exceptional event.

## **7.1 Informality and Urban Planning for Heat**

Cities are at particular risk of extreme heat due to the urban heat island effect which increases temperatures due to the building materials used in highly built-up areas ([Mohajerani et al., 2017](#)). Informal settlements - often lacking in vegetation, public services, and access to passive or active cooling - are particularly exposed ([Climate Centre, 2021](#)). Informal housing is a significant challenge across Central Asian cities, particularly in Tajikistan and Kyrgyzstan, where it accounts for 60-70% of the housing stock in urban areas like Dushanbe and Bishkek ([ADB, 2024](#)). These settlements often lack basic services, are poorly insulated, and lie outside of formal planning zones, increasing vulnerability to heat and other climate risks ([World Bank, 2022](#); [Seitz, 2018](#)). In Uzbekistan and Kazakhstan, informality is more localized, emerging on city fringes due to rapid urban sprawl and limited affordable housing ([Cohen et al., 2025](#); [UNDP, 2024](#)), whereas in Turkmenistan there is limited data on the extent of the issue. In many cities, planning efforts are challenged by limited financial resources, coordination gaps between institutions, and evolving governance frameworks that are still adapting to climate risks ([Sabyrbekov & Overland, 2023](#)).

There is limited integration of disaster risk reduction in spatial and overall development planning in Tajikistan ([ADB, 2024](#)). In Kyrgyzstan and Tajikistan, high levels of housing informality (60-70% of the total housing stock in the latter), particularly in the respective capitals, Bishkek and Dushanbe, complicate centralized planning and heat adaptation as residents may reside outside formal planning and service delivery zones ([ABD, 2024](#); [Seitz, 2018](#)). Poorly insulated homes often made of mud, stone, tin and wood, combined with limited access to regulated cooling and public green spaces, contributes to heightened sensitivity to heat. In Bishkek, rapid and largely unplanned urban growth, driven by high-rise residential construction and road development, has led to significant loss of urban

tree cover over the past two decades, particularly in the southern districts ([Central Asia Climate Portal, 2024](#)). Once regarded as the city's "lungs," these green belts have been fragmented or altogether replaced, plummeting from a Soviet-era norm of 21 m<sup>2</sup> of green space per capita to about 3.5 m<sup>2</sup> in 2021 ([Central Asia Climate Portal, 2024](#)). Green spaces provide important cooling effects within cities through shade and evapotranspiration. Alongside continued reliance on informal, high-emission transport systems, these changes have amplified the urban heat island effect ([Blondin, 2023](#); [Li, 2024](#); [Rekhviashvili & Sgibnev, 2020](#)).

In Uzbekistan, cities like Tashkent face mounting heat stress amid rapid urbanization. Expansion at the urban fringes, often at low density, places pressure on infrastructure systems and complicates the timely delivery of resilience measures ([World Bank, 2022](#)). While a national resilience framework exists, its implementation remains in progress. In Turkmenistan and Uzbekistan, centralized governance structures shape urban planning processes, which can constrain data availability and limit opportunities for community engagement in heat adaptation at the city level ([Cohen et al., 2025](#); [Vakulchuk et al., 2022](#)). Nonetheless, the launch of a \$5 million regional initiative by UNDP and Japan in 2024 is catalyzing multi-country collaboration on disaster risk reduction and resilient urban planning, including in Tashkent, where efforts are advancing in coordination with the Ministry of Ecology to integrate climate adaptation into urban systems ([UNDP, 2024a](#); [UNDP, 2024b](#)).

In Tajikistan, a long-term capacity development program extending from March 2024 to May 2025 is actively training public officials to incorporate climate risks into urban adaptation planning, signaling a gradual strengthening of institutional frameworks ([University of Central Asia, 2024](#)). Kazakhstan has also shown growing initiative, particularly in Astana and Almaty, to integrate climate resilience into planning ([Cohen et al., 2025](#)). However, with a 95% ownership rate, a near absence of rental housing outside Astana and urban housing costs by up to 240% the national average, especially in Almaty, constrain relocation options for vulnerable groups, including climate-affected rural residents seeking urban livelihoods ([Seitz, 2018](#)). Efforts to bridge local and national planning are underway, supported by the development of a National Adaptation Plan (NAP) and pilots in Eastern Kazakhstan. These seek to vertically integrate resilience into sub-national development strategies through institutional reform, capacity building, and continue adjusting the Environmental Code which comprises an eight-step process for climate adaptation ([Government of Kazakhstan, 2019](#)).

Growing multilevel efforts such as the UNDP regional initiative (2024-2017), which promotes cross-border cooperation, climate-informed urban planning, and capacity building in all five Central Asian states, suggest improving conditions for systemic adaptation ([CESDRR, 2024](#); [UNDP, 2024](#)). Platforms like the Central Asian Climate Information Portal (CACIP) are also contributing to shared strategies by facilitating cross-country knowledge exchange, supporting early warning systems, and building local technical capacity for disaster risk reduction and climate resilience in urban areas ([CAREC, 2024](#)). To ensure long-term impact, the Regional Climate Change Adaptation Strategy (2023), endorsed by all five countries, lays out harmonized priorities for climate-resilient urban planning, capacity development, and financing mechanisms, including transboundary climate data systems and citizen-accessible risk tools ([Green Central Asia, 2023](#)). Further, initiatives like CACCC-2025 (more in section 7.4) aim to boost climate finance mobilization by 25% annually to support urban adaptation, highlighting cities as focal points of action in the broader shift toward resilient infrastructure and integrated climate risk management ([CAREC, 2025](#); [CAREC, 2024](#)).

Heat-related vulnerability in the region is not confined to cities. Rural regions, particularly those reliant on climate-sensitive agriculture, face structural exposure.

## 7.2 Agriculture

Agriculture across Central Asia is increasingly affected by rising temperatures, shifting hydrological patterns, and the intensification of extreme heat events. Comprising 5.2-23.3% of the countries' GDP and 20-50% of their work force, agriculture constitutes a critical source of livelihood, food security, and export revenue in the region ([Hamidov et al., 2016](#); [World Bank & ADB, 2021](#); [Sabyrbekov & Overland, 2023](#)). Across most of the affected countries, estimated labor losses across climate-sensitive sectors are highest in agriculture, with 230 million hours in Uzbekistan, 122 million in Tajikistan, 37 million in Kazakhstan, and 6.5 million in Kyrgyzstan in 2023 ([Romanello et al., 2024](#)). Turkmenistan is the exception, where construction suffered more labor loss. Further, the COVID-pandemic has had major impacts on food security and disruptions to livelihoods and the economy in general ([Giap, 2020](#)). Disasters such as the ongoing heatwave can continue to make it harder for livelihood recovery.

The March heatwave coincided with the onset of planting and flowering across much of the region, posing acute risks to crop development. In Kazakhstan, where sowing of spring wheat typically begins in March-April, extreme early-season temperatures can reduce germination rates and soil moisture, especially in rainfed systems ([Sommer et al., 2012](#)). Wheat yields, already projected to decline due to increased heat and drought frequency, are particularly vulnerable ([Narbayan & Pavlova, 2022](#); [Thomas et al., 2021](#)). Crop models suggest potential yield reduction of up to 50% for spring wheat by mid-century under high-emission scenarios ([World Bank & ADB, 2021](#); [Liu et al., 2020](#)). Kazakhstan also faces the region's highest projected cropland exposure to heatwaves due to its large agricultural footprint and northern latitude ([Li et al., 2025](#)).

In the relatively agriculture-dependent Tajikistan and Kyrgyzstan, the timing of the heatwave coincided with the blooming of key export fruit crops such as almonds, apricots, and cherries. High temperatures during flowering can trigger premature flower drop, reducing fruit set and ultimately yield ([Climate Centre, 2021](#)). Farmers in Tajikistan are particularly exposed, with outdoor labor continuing even during extreme heatwaves; a key concern given agriculture's economic role and limited access to protective infrastructure in rural areas ([Red Crescent Society of Tajikistan, 2023](#)). These countries' heavy dependence on glacier-fed irrigation systems adds an additional layer of sensitivity, as altered snowmelt timing reduces water availability during the peak growing season ([GIZ, 2024a](#); [Reyer et al., 2017](#)).

In Uzbekistan and Turkmenistan, cotton production, dependent on early-season irrigation, is increasingly at risk. Early snowmelt reduces spring water availability, while high heat accelerates evapotranspiration and soil salinization, especially in arid regions including the deserts and dry lowlands of Turkmenistan, Uzbekistan, southern Kazakhstan, southwestern Tajikistan, and interior valleys of Kyrgyzstan ([GIZ, 2024a](#)). Without improved water efficiency, crop productivity is expected to decline sharply ([Thomas et al., 2021](#); [Cohen et al., 2025](#)).

Adaptation measures under consideration across the region include shifting planting calendars (such as starting earlier in the spring to avoid peak summer), adopting heat-tolerant varieties (such as alatau,

zhetsu, and karakalpakskaya), and investing in climate-resilient irrigation systems (such as low-pressure sprinkler systems and drip irrigation) ([Climate Centre, 2021](#); [Thomas et al., 2021](#)). However, implementation varies widely depending on access to technical resources, infrastructure, and support systems, especially among smallholder and rainfed farming communities. These differences reflect broader disparities in climate governance. While countries like Kazakhstan and Tajikistan have integrated adaptation priorities into national agricultural and climate frameworks, enforcement and coordination remain limited ([World Bank, 2022](#); [Sabyrbekov et al., 2023](#)). Kyrgyzstan and Tajikistan have developed Early Action Protocols for heat and investing in anticipatory planning mechanisms with cross-sectoral participation, but institutional capacity and reliance on external financing remain key constraints ([IFRC, 2023](#); [WFP, 2023a](#); [Red Crescent Society of Tajikistan, 2023](#)).

The pressures facing agriculture under rising temperatures mirror broader vulnerabilities across critical services - shaped by environmental stressors, outdated infrastructure, and uneven access.

### **7.3 Water, Electricity, and Health Systems**

Central Asia's essential service systems are increasingly under pressure from rising temperatures, glacier melt, and shifting hydrological patterns. In Kazakhstan, water stress is mounting due to shrinking glaciers and reliance on transboundary rivers such as the Ili and Ural ([Narbayev & Pavlova, 2022](#)). Tensions over shared water resources are growing across the region, as upstream countries like Kyrgyzstan and Tajikistan prioritize hydropower while downstream neighbors, especially Uzbekistan and Turkmenistan, depend on summer river flows for irrigation. Disputes over major rivers like the Syr Darya and Ama Darya are longstanding, and climate change is intensifying these dynamics by making water flows more unpredictable and competition more acute ([Russell, 2018](#); [Idrisov, 2023](#)). Recent initiatives like joint hydrotechnical projects between Uzbekistan and Turkmenistan aim to mitigate tensions but face obstacles due to differing needs ([Sarymbetova, 2025](#)).

Further, nearly 40% of irrigation water and 55% of drinking water are lost due to aging infrastructure ([Cohen et al., 2025](#)), with rural areas experiencing limited access. While urban centres like Almaty are relatively well-serviced, they remain vulnerable to combined heat and water disruptions ([GIZ, 2024a](#)). Electricity demand is rising with increased cooling needs, prompting a shift toward renewables, supported by green energy projects and international partnerships ([Climate Centre, 2021](#); [Broomandi et al., 2024](#)). Meanwhile, health systems, especially outside cities, are only partially equipped for sustained heat impacts ([Legro, 2024](#)). Many rural health clinics lack cooling systems, backup electricity, or even reliable access to water, which are critical during heatwaves ([Legro, 2024](#)). Further, health workers in remote areas often lack training on how to recognize and manage heat-related illnesses such as heatstroke or dehydration, especially in vulnerable groups. Kazakhstan has seen increases in all-cause and cardiovascular mortality during past heatwaves, particularly in western and southern regions, underscoring the health system's limited capacity for heat response outside major urban centers ([Broomandi et al., 2024](#)).

Uzbekistan draws approximately 80% of its water from upstream neighbors, rendering the system highly vulnerable to regional dynamics and climate-induced supply shifts ([Cohen et al., 2025](#)). Outdated infrastructure and high agricultural demand strain both water and energy sectors ([Atlantic Council, 2025](#)). Around 30% of the rural population lacks reliable water access, often relying on

unsafe sources ([Atlantic Council, 2025](#)). Heatwaves have compounded risks for health systems, particularly in cities like Tashkent, where infrastructure is stretched ([World Bank, 2022](#)).

Kyrgyzstan, despite abundant water resources, faces challenges with delivery and quality, particularly in rural areas. Rapid urban growth in Bishkek has outpaced infrastructure capacity, leading to water shortages during recent heat events ([Atlantic Council, 2025](#)). Only 58% of rural residents have piped water, and up to one-third of piped systems do not meet sanitary standards ([SIWI, 2017](#); [World Bank, 2024](#)). While supported by international efforts to expand access and modernize networks, challenges persist, including aging Soviet-era infrastructure and seasonal variability in hydropower-dependent electricity ([Muratalieva, 2022](#); [Cohen et al., 2025](#)).

Tajikistan holds the region's greatest water reserves but remains vulnerable due to infrastructure limitations, climate-driven glacier loss, and heavy reliance on hydropower ([Narbayev & Pavlova, 2022](#)). Access to piped water remains low in rural areas, and the health system faces capacity constraints in managing heat-related illness ([Legro, 2024](#)). Recent Early Action Protocols (EAPs) in Tajikistan have identified pregnant women, people with disabilities, and older adults living alone as highly vulnerable to heat-related illness, especially where access to water, cooling, and basic health services is limited during heatwaves ([Red Crescent Society of Tajikistan, 2023](#)).

Turkmenistan faces chronic water shortages which stems from its geography, as over 80% of the country is desert, relying heavily on the Amu Darya river for irrigation, despite being a downstream state with little control over water flows ([Cohen et al., 2025](#)). Much of this water is lost due to poorly maintained irrigation canals, with leakage losses exceeding 50% in both agriculture and drinking water systems ([Cohen et al., 2025](#)). Meanwhile, rural electrification remains limited and outdated, notably in sparsely populated desert areas. While national electricity access is high on paper, in practice, many rural communities lack stable and modern energy services, such as air conditioning and refrigeration which are crucial under rising heat extremes ([Mehta et al., 2021](#); [Narbayev & Pavlova, 2022](#); [GIZ, 2024a](#)).

These cross-sector vulnerabilities point to a common need for coordinated planning. The following section examines how institutions across the region are beginning to address heat risk through evolving governance frameworks.

## **7.4 Heat Risk Governance**

Heat risk governance across the region remains in a formative stage, shaped by uneven institutional capacities, data limitations, and evolving coordination frameworks. While all countries acknowledge climate threats, adaptation strategies targeting extreme heat are often nascent, fragmented, or embedded within broader climate and disaster risk agendas ([World Bank & ADB, 2021](#)).

However, the 2023 Regional Climate Change Adaptation Strategy, developed under the Green Central Asia Initiative, marks a pivotal shift by outlining a region-wide roadmap to climate resilience through 2030. The strategy supports joint political dialogue, promotes harmonized climate risk management, and mandates a shared Secretariat and knowledge hub to facilitate coordination on water, energy, and ecosystem protection ([Green Central Asia, 2023](#)). Strategic objectives including building capacity for

adaptation planning, developing national and regional action plans, and scaling access to climate finance. Complementing this, the Central Asian Climate Information Platform (CACIP) fosters regional cooperation through open data sharing, technical training, and promotion of sustainable infrastructure and water systems, while enabling city-level officials to plan for climate risks ([CAREC, 2024](#)). Further regional alignment is supported through the CAREC Climate Change Action Plan (2025-2027) which focuses on glacier risk assessments, water forecasting systems, and climate-adaptive infrastructure, reinforcing links between science, policy, and planning ([CAREC, 2025](#)).

Kazakhstan has made notable strides in integrating heat and water stress into national frameworks, including recent environmental strategies and its active participation in regional platforms such as IFAS and GIZ-led climate risk assessments ([GIZ, 2024a](#); [Cohen et al., 2025](#)). The country has also begun strengthening its disaster loss data systems through the Desinventar Sendai platform, which supports national heat risk tracking and aligns with the Sendai Framework ([UNDRR & ADPC, 2023](#)). Ongoing efforts to develop Kazakhstan's National Adaptation Plan (NAP) aim to ensure vertical integration of climate priorities across national and sub-national levels. Earlier pilot work in Eastern Kazakhstan provided a regional adaptation blueprint, and current reforms focus on aligning local planning with national strategy through institutional reform and cross-sector coordination ([Government of Kazakhstan, 2019](#)). While adaptation enforcement still remains limited, efforts to contextualize global best practices (such as the integration of climate adaptation into Kazakhstan's national planning system and the adoption of ecosystem-based adaptation approaches in Tajikistan) and develop science-based, regionally grounded approaches signal growing momentum ([Reyer et al., 2017](#); [Sabyrbekov et al., 2023](#)). The establishment of dedicated climate institutions, such as government ministries and agencies and regional cooperation mechanisms such as IFAS and CAREC, and moderate access to green finance are enabling further planning, although research emphasizes that innovation systems remain under development ([Sabyrbekov & Overland, 2023](#)).

At the national level, Kyrgyzstan is also developing a NAP while participating actively in regional frameworks such as Green Central Asia and CACIP ([Green Central Asia, 2023](#); [CAREC, 2024](#)). Kyrgyzstan has enhanced its hydromet and disaster risk management systems with international support, including high-altitude monitoring and early warning system upgrades such as the restoration and technical upgrade of meteorological observational networks ([GIZ, 2024b](#)). Kyrgyzstan has also operationalized heat-specific Early Action Protocols (EAPs) through Forecast-based Financing (FbF), coordinated with the Ministry of Emergency Situations, and activated with four-day lead times based on multi-day heat forecasts ([IFRC, 2022](#); [Red Crescent society of Kyrgyzstan, 2019](#)). Parallel efforts led by World Food Programme (WFP) are embedding anticipatory action principles into Kyrgyzstan's national disaster risk management system, with institutional buy-in from emergency, agriculture, and social protection ministries ([WFP, 2023a](#); [2023b](#)). Across said programmes, early actions include cash and voucher assistance, air conditioning installed in care facilities to keep room temperatures below 25C, public awareness and first aid campaigns, and more.

Tajikistan engages actively in regional climate planning and has comprehensive policy frameworks such as the Agriculture Sector Development Program (ASDP) 2030, which outlines structural reforms aimed at strengthening food system resilience including investment in early warning and emergency preparedness to address heat stress ([World Bank, 2022](#)). Still, implementation remains limited and reliant on donor initiatives ([Khakimov et al., 2024](#); [Narbayep & Pavlova, 2022](#)). Tajikistan's adoption of FbF and development of EAPs for heat and cold waves illustrate growing national capacity to

operationalize anticipatory action. Implemented through cross-sectoral coordination with the Tajik Hydromet, disaster agencies, and local authorities, the approach emphasizes timely, localized response ([Red Crescent Society of Tajikistan, 2023](#)). EAPs in Tajikistan rely on forecasts with 3-5 day lead times to activate responses to extreme temperature events, including early actions such as distributing drinking water supplies, hats, caps and umbrellas, and public awareness campaigns ([IFRC, 2023](#); [Red Crescent Society of Tajikistan, 2023](#)). These FbF initiatives have contributed to improved early warning linkages, local capacity-building, multi-hazard coordination, local responder training, and public awareness, especially in rural high-risk areas where access to services remain limited ([Anticipation Hub, 2023](#); [IFRC, 2023](#); [Red Crescent Society of Tajikistan, 2023](#)). Further, they have enhanced GIS-based planning, responder readiness, and inclusion of vulnerable communities in preparedness efforts, offering scalable lessons for heat-specific governance. Despite progress, research suggests that coordination between sectors remains a key area for development, particularly under increasing water-energy pressures ([Cohen et al., 2025](#); [Narbayev & Pavlova, 2022](#)).

Uzbekistan is undergoing a shift toward more integrated climate governance, now implementing a regional urban resilience initiative in partnership with UNDP under the Ministry of Ecology, Environmental Protection and Climate Change, integrating heat adaptation into urban policy and leveraging Japan's technical support in climate-resilient infrastructure ([UNDP, 2024](#)). 10 years ago the country piloted a Heat Wave Action Plan with WHO and UNDP, establishing early warning systems, defining temperature thresholds, and training health workers ([WHO & UNDP, 2015](#)). UNICEF ([2024](#)) has since supported efforts to expand heat resilience through social protection, insurance, and climate-proofing of schools and clinics. Initiatives in urban resilience, stakeholder training, and transboundary cooperation are underway, notably in Tashkent ([World Bank, 2022](#); [GIZ, 2024c](#)).

Turkmenistan, while still early in internal planning, has signaled greater engagement through participation in region-wide initiatives including the upcoming Central Asia Climate Change Conference (CACCC-2025) which will emphasize adaptation and climate finance with a special focus on urban vulnerabilities ([Yakulchuk et al., 2022](#); [Sabyrbekov & Overland, 2023](#); [CAREC, 2025](#)).

Across Central Asia, early warning systems, hazard mapping, and capacity-building initiatives are expanding through regional and donor-supported programmes. Notably, the Asian Development Bank's 2025-2030 Climate Action Roadmap for Central and West Asia complements these efforts by prioritizing urban climate resilience, regional infrastructure, and policy coherence ([ADB, 2024](#)). However, institutional coordination, sectoral integration, and long-term heat-specific adaptation remain priorities for strengthening resilience ([Issyk-Kul Forum, 2024](#); [GIZ, 2024a](#)).

## **V&E Conclusions**

The recent heatwave across Central Asia was unprecedented in timing and intensity, and this analysis reveals that in today's climate it is already 1.3C warmer and no longer rare. As the planet continues to warm, this increase will continue. Rapid warming conditions, especially in early spring, compound risk in both urban and rural settings. Urban centers like Bishkek and Tashkent face intensified heat due to rapid, often informal development, reduced green cover, and limited integration of heat risk in planning. Rural areas remain highly exposed due to often limited, under-resourced and

climate-sensitive infrastructure and heavy reliance on weather-dependent agriculture - particularly during critical periods like flowering and planting, during which the March heatwave hit.

Essential service systems, notably water, electricity, and health, are strained by aging infrastructure and rising demand, while reliance on shared water sources (like the Amu Darya and Syr Darya rivers) adds political and logistical complexity to adaptation planning and coordinated responses to weather and climate extremes. Despite considerable adaptation efforts on regional, national and city levels emerging in recent years, governance remains uneven with heat-specific strategies still nascent.

Critically, the hazard analysis finds that observed temperature trends outpace model projections, particularly for early-season extremes. This gap signals that existing models may underestimate near-term risks, which poses challenges for adaptation planning that relies on them. In response, strategies must be both anticipatory and flexible, designed not only around expected changes but also stress-tested for worst-case and outlier scenarios. Planning should address both the growing intensity and seasonal shifts of heat. This requires mainstreaming heat risk into urban development, agricultural calendars, and public infrastructure design, with a focus on systems that can evolve as new evidence emerges. Further, it is key to prioritize informal contexts, rural communities, and critical services where many at-risk groups live and work, and where exposure is highest. Adaptation must also account for compounding risks, including glacier loss and water scarcity, which intensify the impacts of heat across agriculture, energy, and public health systems. Regionally, adaptation will also hinge on enhanced coordination, from transboundary water governance to shared climate data platforms. As the climate signal strengthens, adaptation must not only scale but evolve - linking forecasts and foresight with social protection and long-term development planning to ensure the most vulnerable are not left behind. Achieving this will require context-specific measures tailored to diverse geographies, governance systems, and social conditions across the region.

### **Data availability**

All time series used in the attribution analysis are available via the Climate Explorer.

### **References**

All references are given as hyperlinks in the text.

## Appendix

### A.1 Trends in observed data

T<sub>max</sub>

Station (Country)	Event		Trend with GMST	
	Magnitude (C)	Return period	Probability ratio	Change in intensity (C)
Dzhalal Abad (Kyrgyzstan)	23.82	3	<b>31.20</b> (6.36 - inf)	<b>5.97</b> (2.91 - 8.90)
Fergana (Uzbekistan)	22.97	3	<b>6.67</b> (2.07 - 36.17)	<b>3.76</b> (1.33 - 6.28)
Kurgan-Tyube (Tajikistan)	27.28	3	<b>30.65</b> (6.14 - inf)	<b>4.27</b> (2.40 - 6.16)
Kazalinsk (Kazakhstan)	20.11	3	<b>31.13</b> (6.40 - inf)	<b>8.13</b> (4.28 - 11.62)
Namangan (Uzbekistan)	23.64	3	<b>32.77</b> (3.67 - inf)	<b>5.42</b> (2.55 - 9.49)
Saragt (Turkmenistan)	27.71	3	3.14 (0.96 - 23.95)	2.49 (-0.083 - 5.01)
Turkestan (Kazakhstan)	23.22	3	<b>5.77</b> (1.86 - 30.17)	<b>3.78</b> (1.46 - 6.33)

Table A.1: Magnitude of the 3-year Tx5day event in several local stations, as well as the probability ratio and change in magnitude for such events from the preindustrial (1.3 C cooler) to present climate.

T<sub>min</sub>

Station (Country)	Event		Trend with GMST	
	Magnitude (C)	Return period	Probability ratio	Change in intensity (C)
Dzhalal Abad (Kyrgyzstan)	8.14	2	<b>26.22</b> (4.41 - inf)	<b>3.69</b> (1.66 - 5.54)
Kurgan-Tyube (Tajikistan)	11.28	2	2.07 (0.70 - 7.30)	1.25 (-0.54 - 2.89)

Kazalinsk (Kazakhstan)	1.06	2	1.13 (0.50 - 2.56)	0.45 (-2.51 - 3.36)
Saragt (Turkmenistan)	10.42	2	1.51 (0.30 - 4.75)	1.15 (-2.65 - 4.63)
Turkestan (Kazakhstan)	5.79	2	1.33 (0.55 - 3.11)	0.84 (-1.53 - 3.55)

Table A.2: Magnitude of the 2-year  $T_{n5day}$  event in several local stations, as well as the probability ratio and change in magnitude for such events from the preindustrial (1.3 C cooler) to present climate.

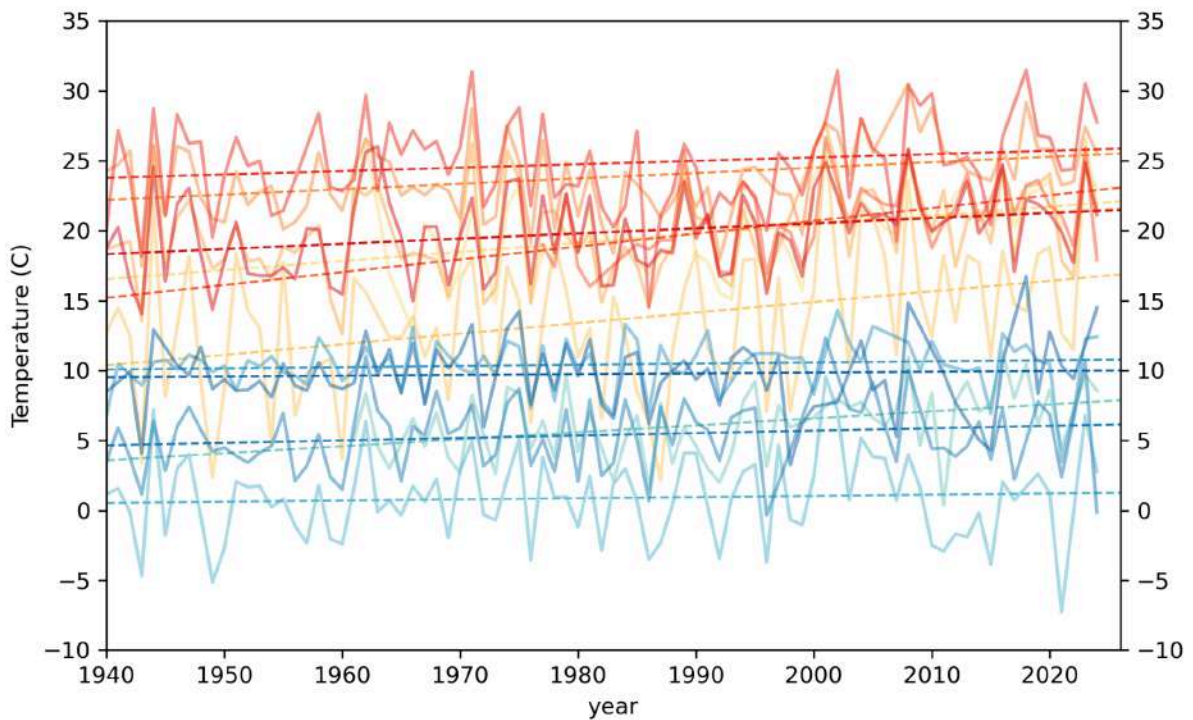


Figure A.1: Time series of local station data for  $T_{x5day}$  (oranges) and  $T_{n5day}$  (blues). The linear best fit to each time series over time is shown as a dashed line.

### 1-day March maxima

Variable	Dataset	Event		Trend	
		Magnitude (C)	Return period	Probability ratio	Change in intensity (C)
Tmax	MSWX	24.88	1.72 (1.22 - 2.62)	<b>3983.9</b> <b>(36.98 - inf)</b>	<b>12.32</b> <b>(9.04 - 16.85)</b>
	CPC	27.12	2.03	<b>8.15E+06</b>	<b>12.40</b>

			(1.35 - 3.47)	<b>(49.57 - inf)</b>	<b>(9.00 - 17.09)</b>
	ERA5	23.17	2	<b>29.27</b> <b>(8.21 - 7.18E+05)</b>	<b>6.39</b> <b>(4.04 - 9.06)</b>
Tmin	MSWX	11.62	2.01 (1.30 - 3.86)	<b>Inf</b> <b>(693.50 - inf)</b>	<b>7.92</b> <b>(4.80 - 11.91)</b>
	CPC	10.29	1.31 (1.08 - 1.64)	<b>Inf</b> <b>(93.54 - inf)</b>	<b>7.19</b> <b>(4.71 - 10.69)</b>
	ERA5	8.61	2	<b>103.92</b> <b>(15.38 - inf)</b>	<b>4.63</b> <b>(2.90 - 6.40)</b>

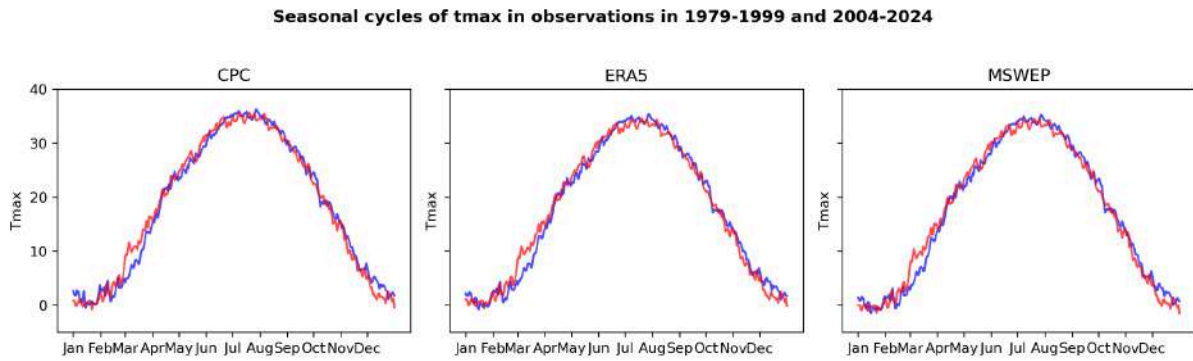
Table A.3: Estimated return periods of Tx5day and Tn5day events over the Central Asia region in the three reanalysis datasets used in this study, as well as probability ratio and change in magnitude with increasing GMST. Statistically significant trends are highlighted in **bold** font.

#### Gridded data annual 5-day maxima

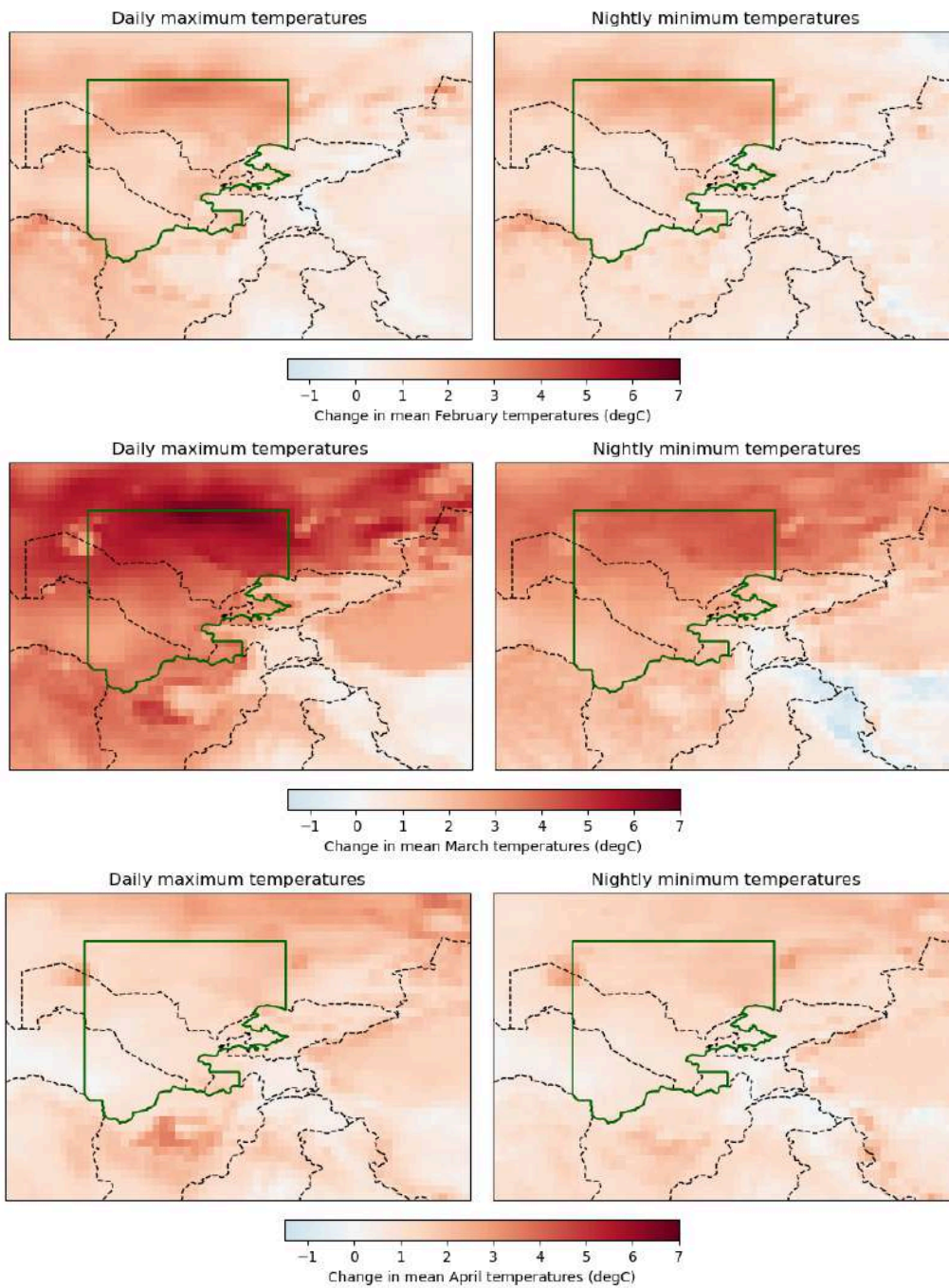
Variable	Dataset	Event		Trend	
		Magnitude (C)	Return period	Probability ratio	Change in intensity (C)
Tx5day	MSWX	39.79	3	<b>Inf</b> <b>(1.37 - inf)</b>	<b>2.49</b> <b>(0.33 - 4.11)</b>
	CPC	41.00	3	<b>Inf</b> <b>(4.92 - inf)</b>	<b>3.19</b> <b>(1.19 - 4.87)</b>
	ERA5	39.55	3	<b>8.47</b> <b>(2.13 - inf)</b>	<b>1.70</b> <b>(0.62 - 2.87)</b>
Tn5day	MSWX	26.41	3	<b>Inf</b> <b>(355.01 - inf)</b>	<b>2.75</b> <b>(1.51 - 3.88)</b>
	CPC	24.38	3	<b>46.37</b> <b>(1.53 - inf)</b>	<b>1.45</b> <b>(0.22 - 2.94)</b>
	ERA5	25.69	3	<b>145.68</b> <b>(8.62 - inf)</b>	<b>1.91</b> <b>(1.11 - 2.90)</b>

Table A.4: Estimated return periods of Tx5day and Tn5day events over the Central Asia region in the three reanalysis datasets used in this study, as well as probability ratio and change in magnitude with increasing GMST. Statistically significant trends are highlighted in **bold** font.

## A.2 March temperature change



*Figure A.2: Seasonal cycles of daily maximum temperatures in three observational and reanalysis datasets. The blue line shows the 1979-1999 average seasonal cycle, and the red line shows the 2004-2024 average seasonal cycle with the mean difference between the two cycles subtracted.*



*Figure A.3: Maps of the change in daily maximum (left) and daily minimum (right) temperatures in the months of February (top), March (middle) and April (bottom) in ERA5 data, between the periods 1979-1999 and 2000-2020.*

Seasonal cycles of tmax in CMIP6 in 1850-1880 and 2070-2100

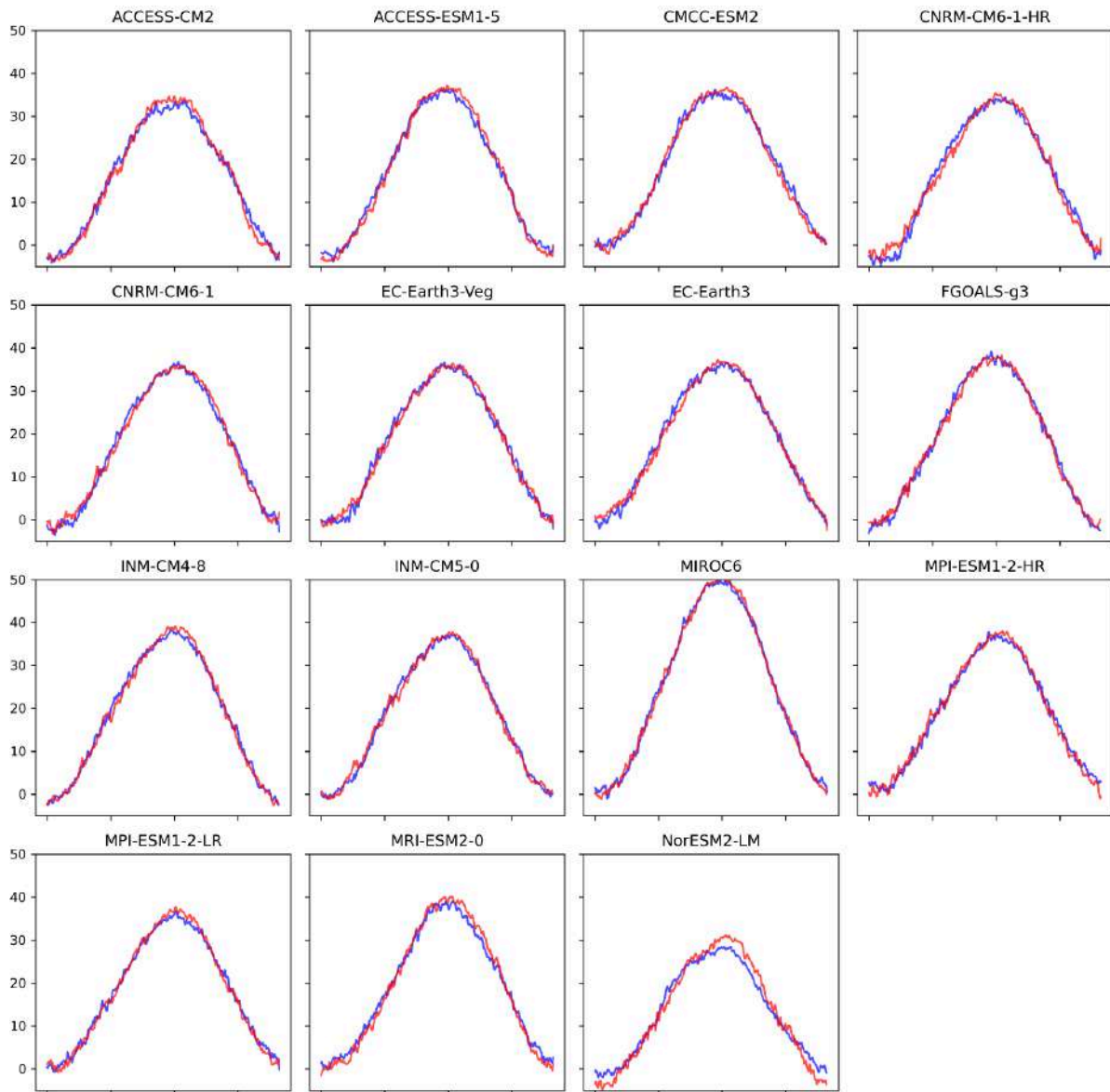


Figure A.4: As for Fig. A.2, but for CMIP6 models and the periods 1850-1880 and 2070-2100, with the mean difference subtracted.

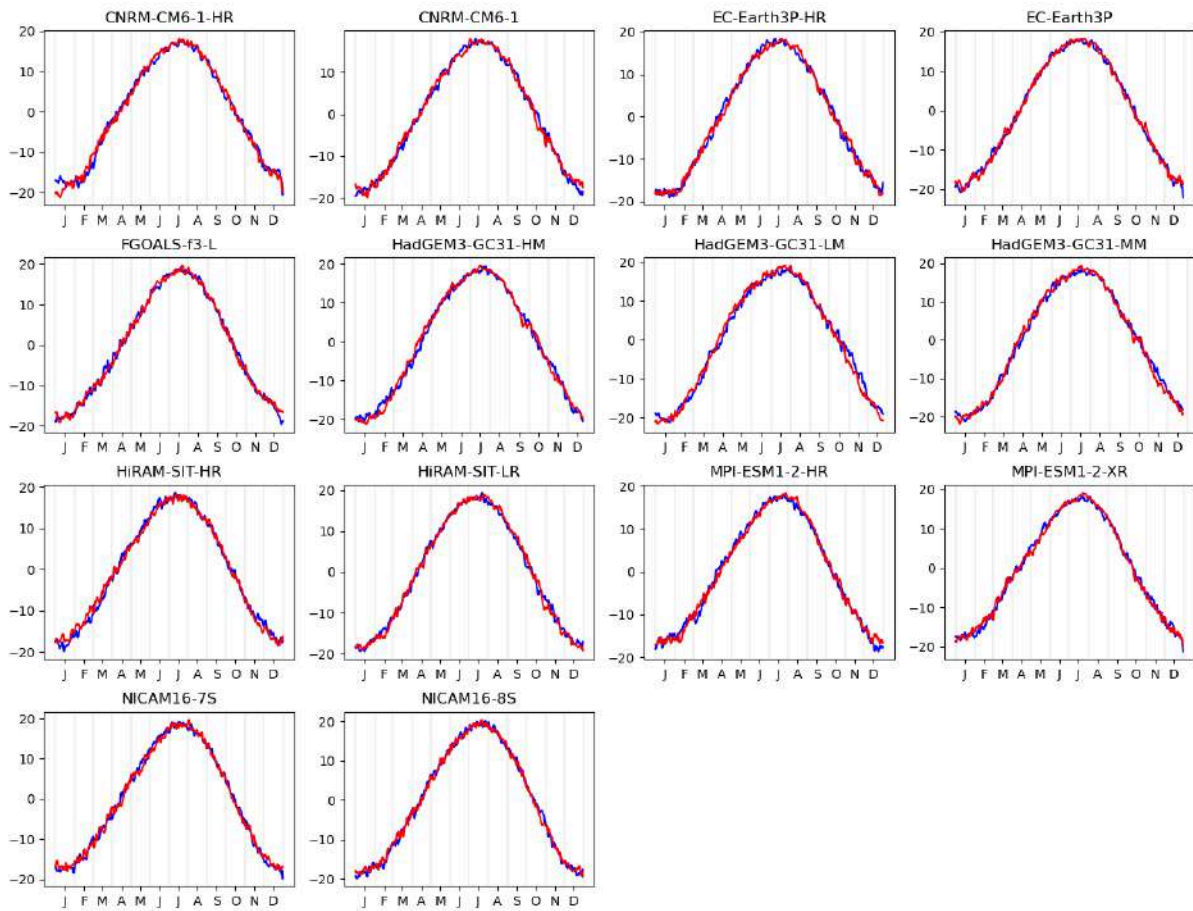


Figure A.5: As for Figs. A.3&A.4, but for HighResMIP models and the periods 1950-1980 and 2020-2050, with the mean difference subtracted.

### A.3 Model evaluation figures

#### A.3.1 CMIP6

Spatial pattern of tmax in Observations & CMIP6

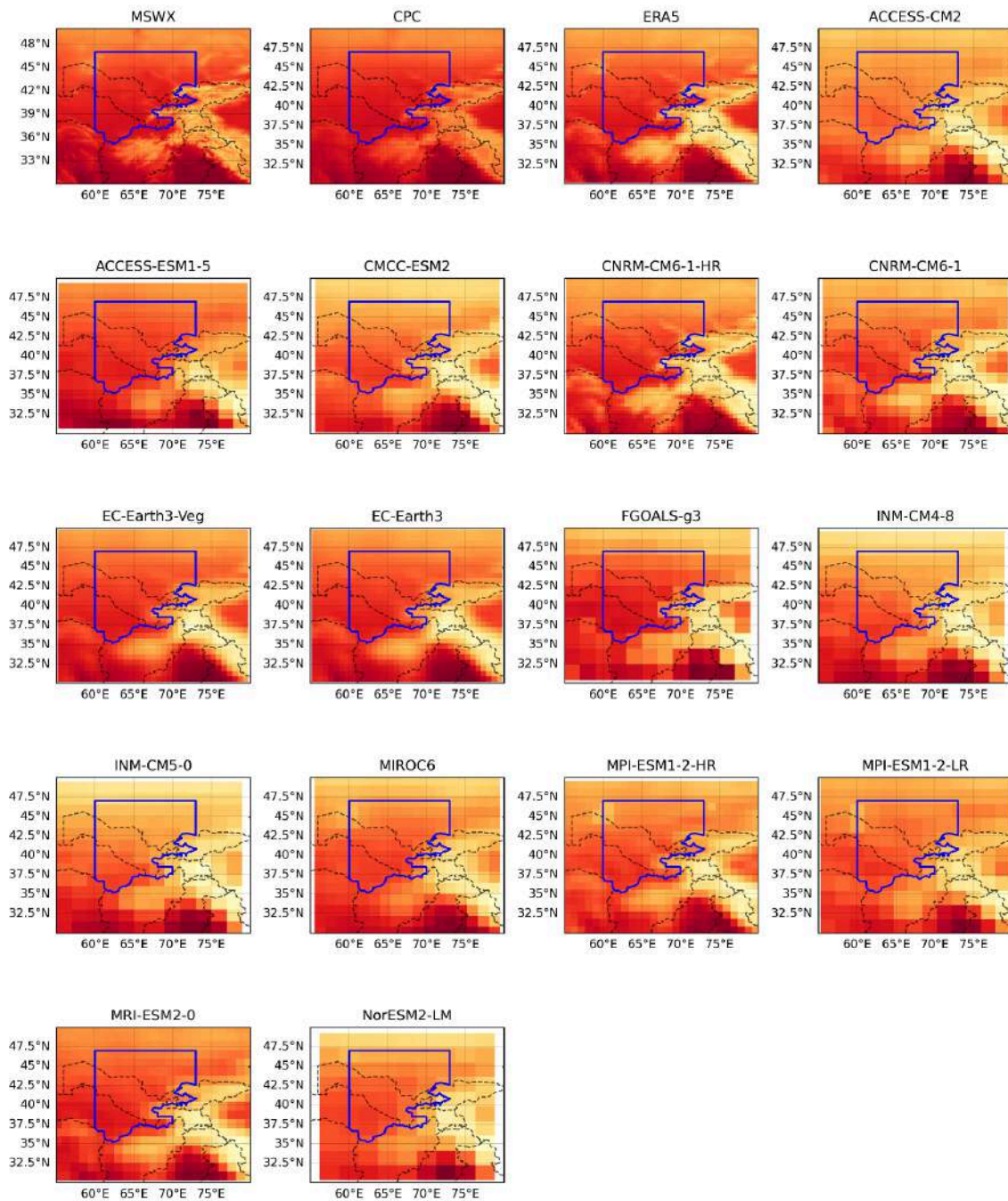


Figure A.6: Spatial patterns of March daily maximum temperatures in observations and CMIP6 models. The study region is highlighted in blue.

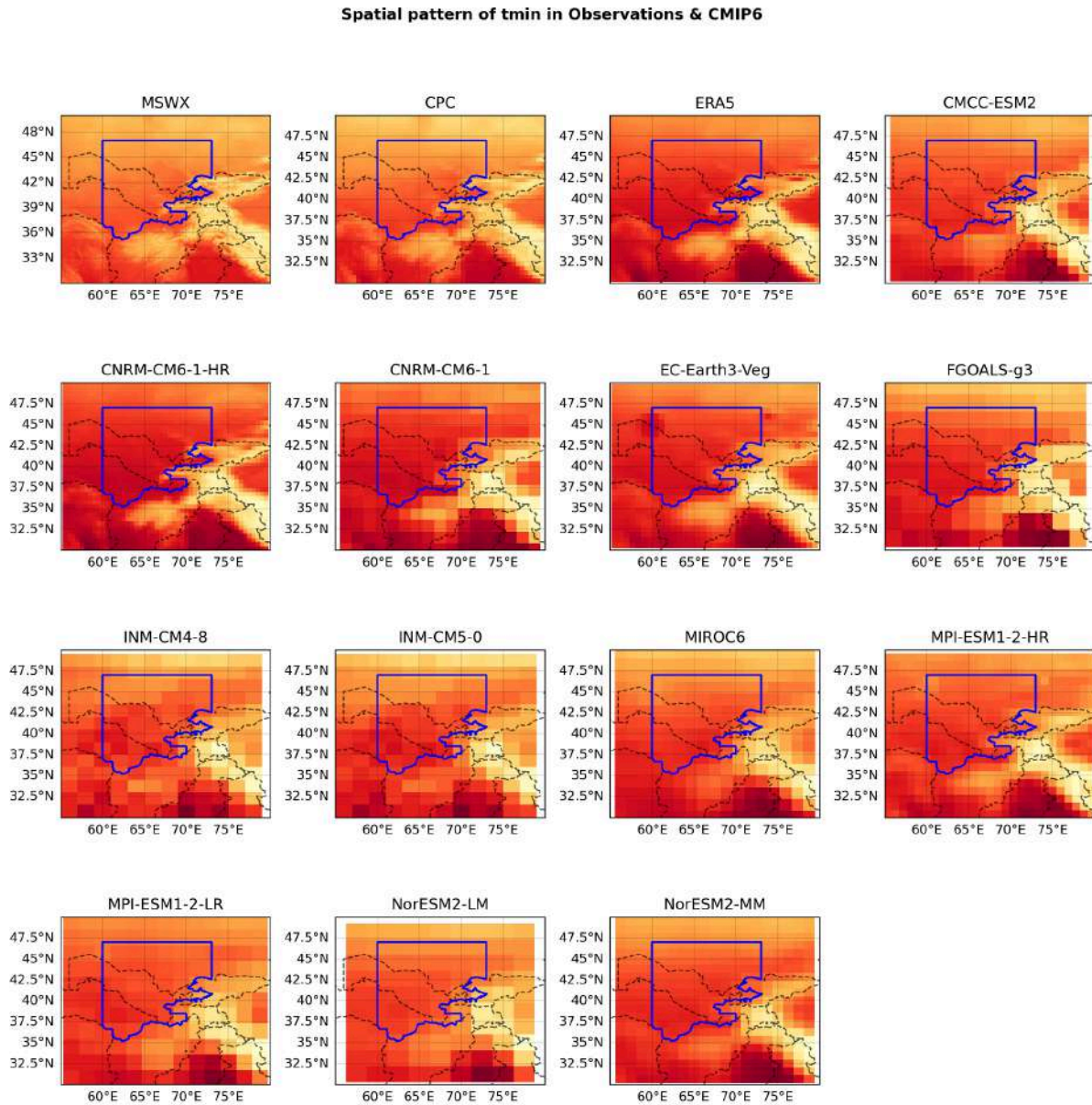


Figure A.7: Spatial patterns of March daily minimum temperatures in observations and CMIP6 models. The study region is highlighted in blue.

### Seasonal cycles of tmax in Observations & CMIP6

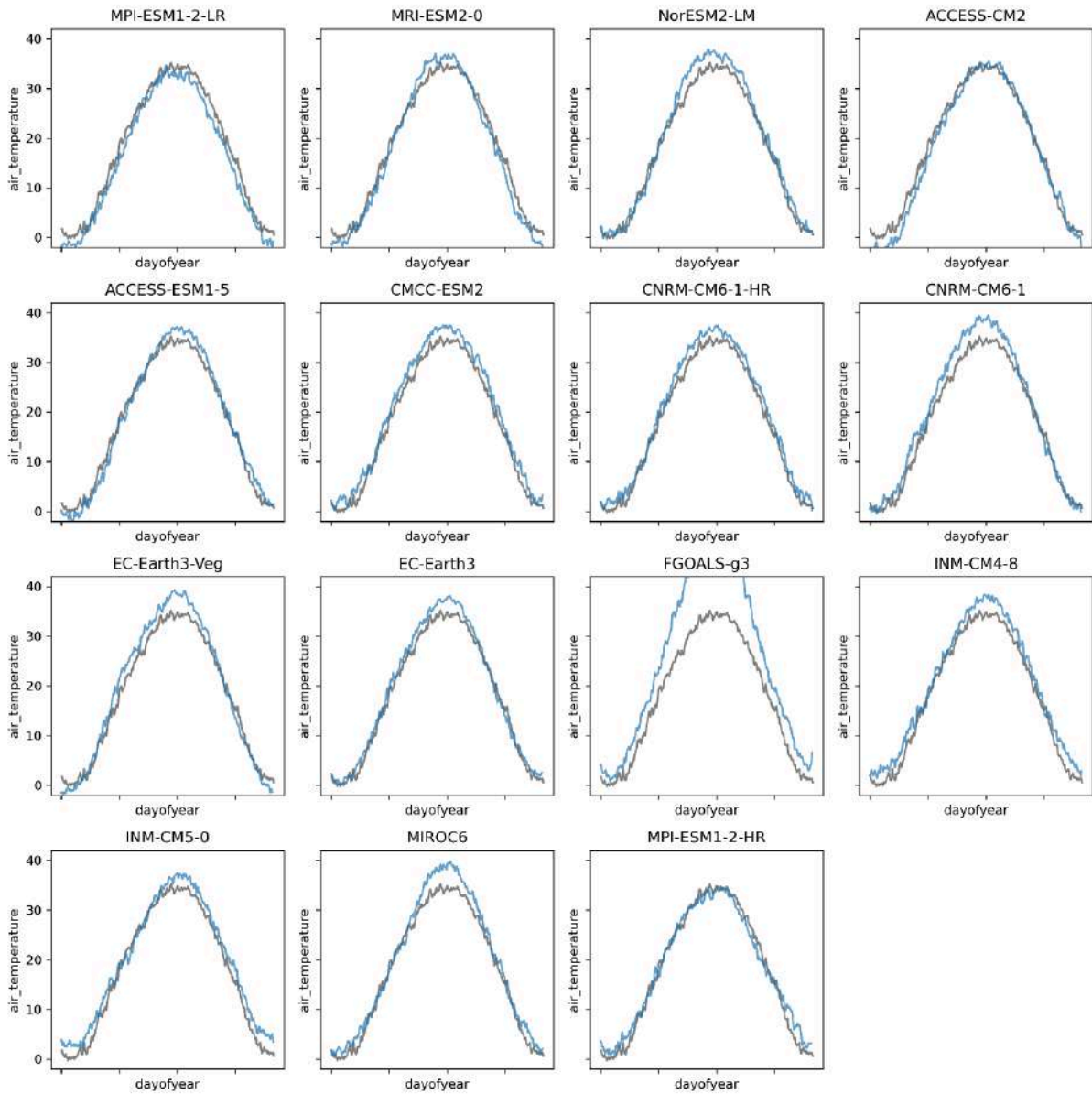


Figure A.8: Seasonal cycles of daily maximum temperatures in observations (MSWX), shown in black, and CMIP6 models, shown in blue.

### Seasonal cycles of tmin in Observations & CMIP6

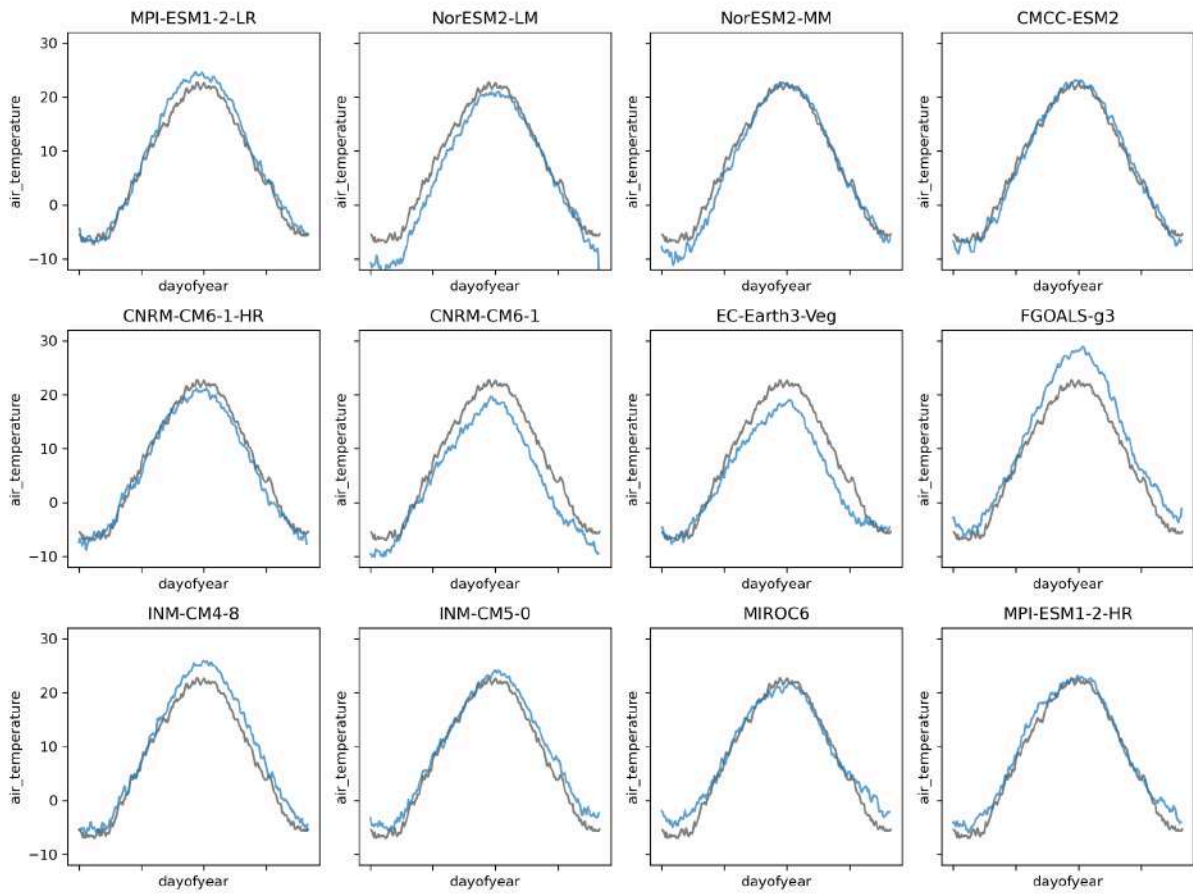


Figure A.9: Seasonal cycles of daily minimum temperatures in observations (MSWX), shown in black, and CMIP6 models, shown in blue.

### A.3.1 HighResMIP

Spatial pattern of tmax in Observations & HighResMIP

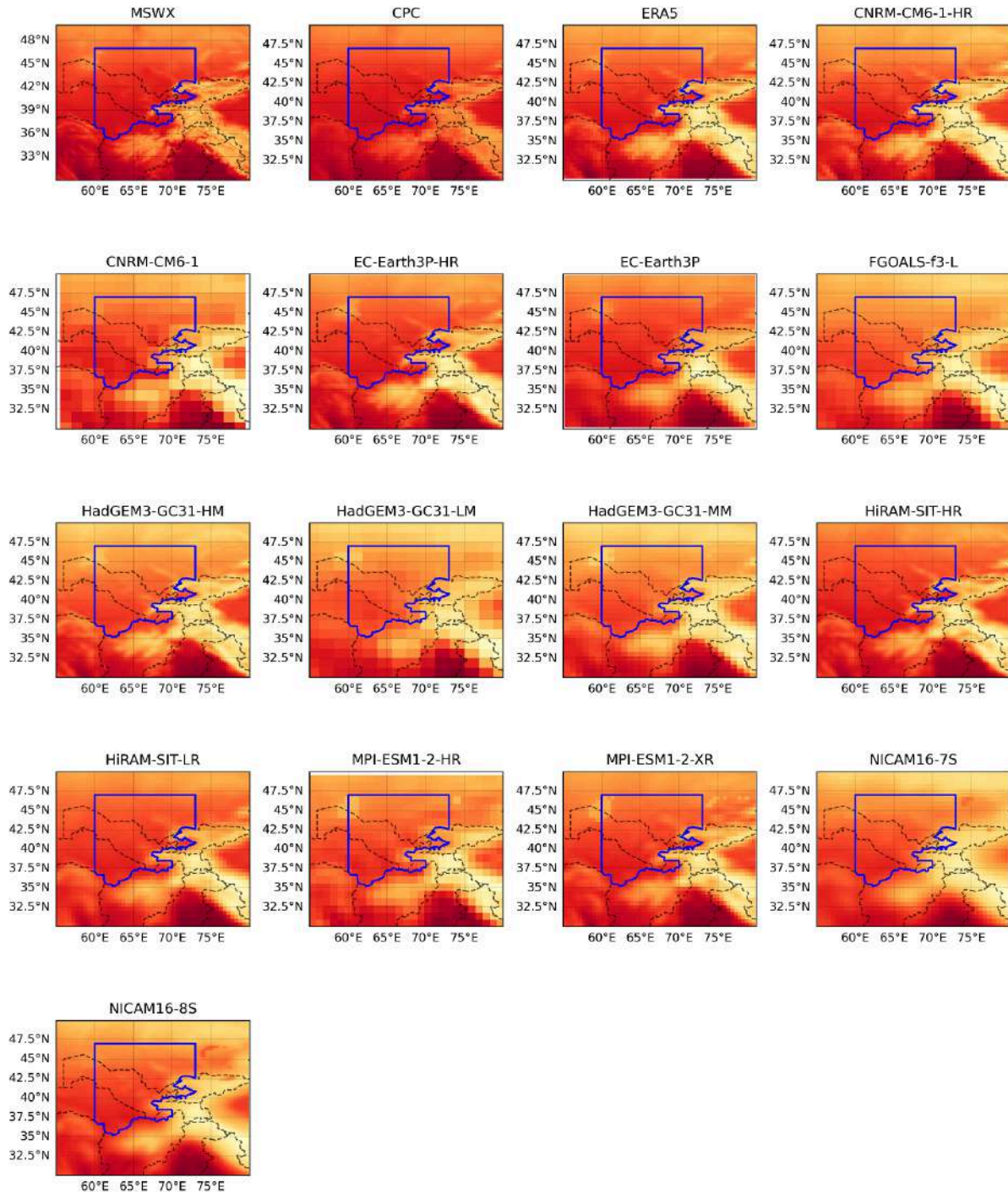


Figure A.10: Spatial patterns of March daily maximum temperatures in observations and HighResMIP models. The study region is highlighted in blue.

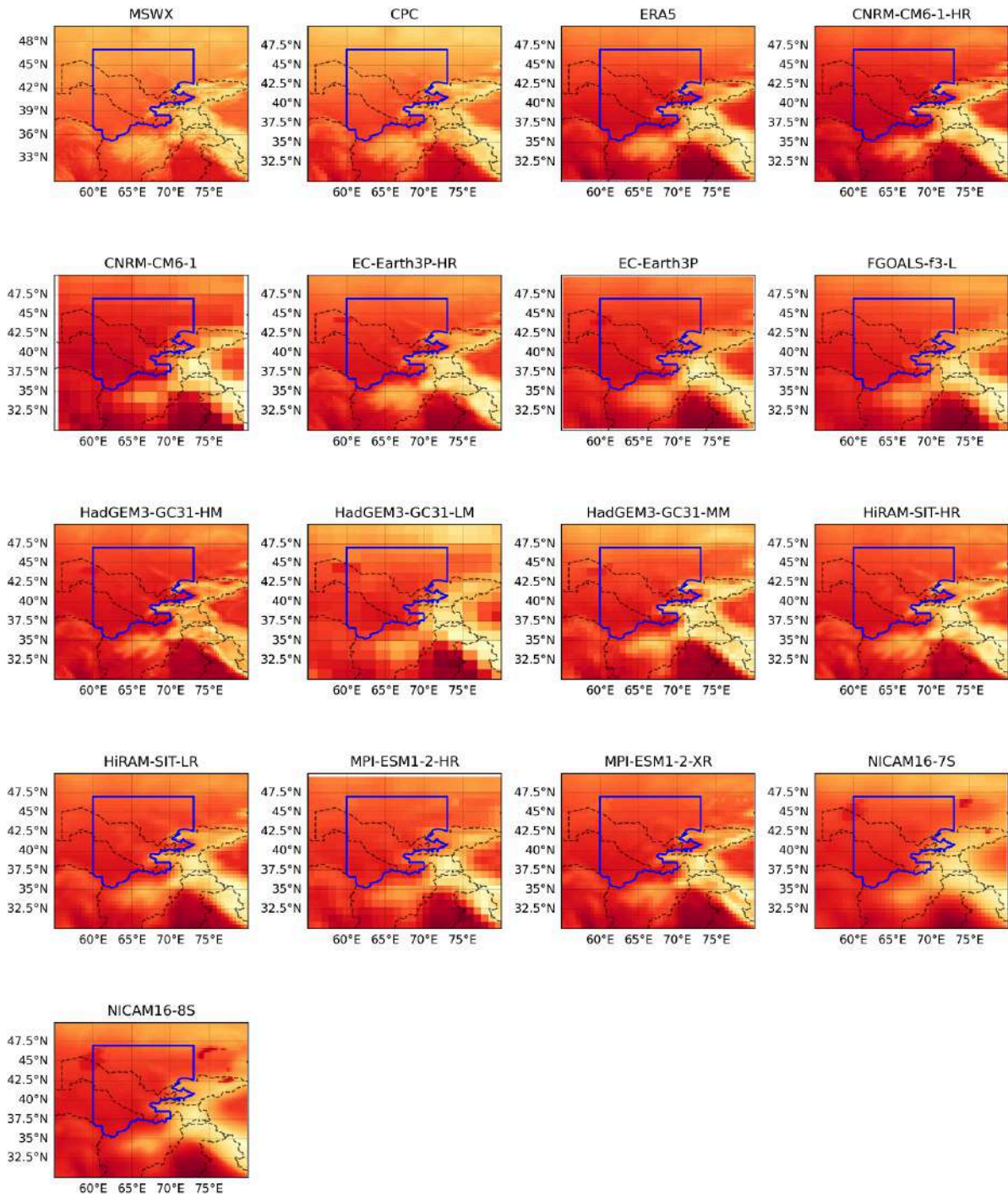
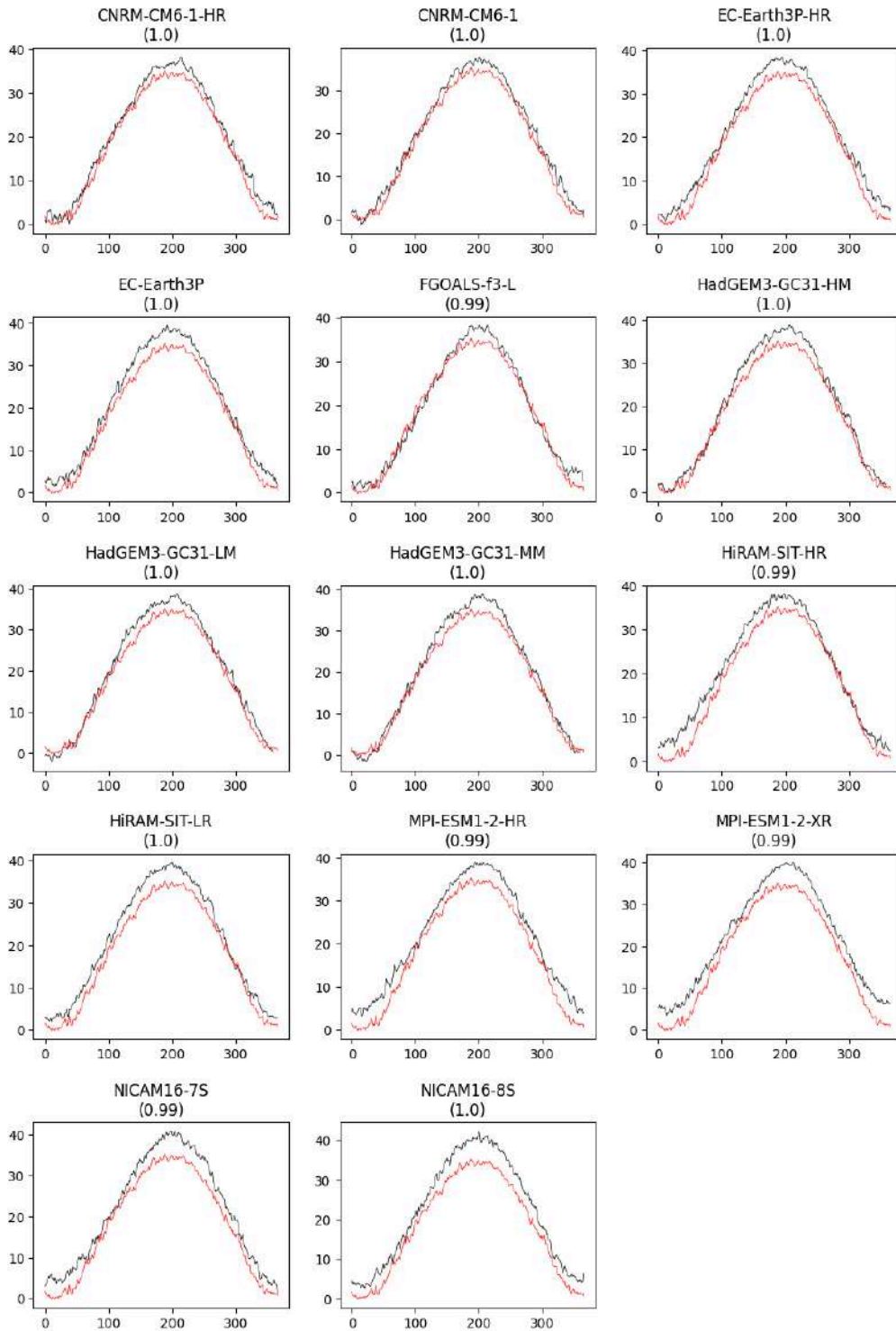


Figure A.11: Spatial patterns of March daily minimum temperatures in observations and HighResMIP models. The study region is highlighted in blue.

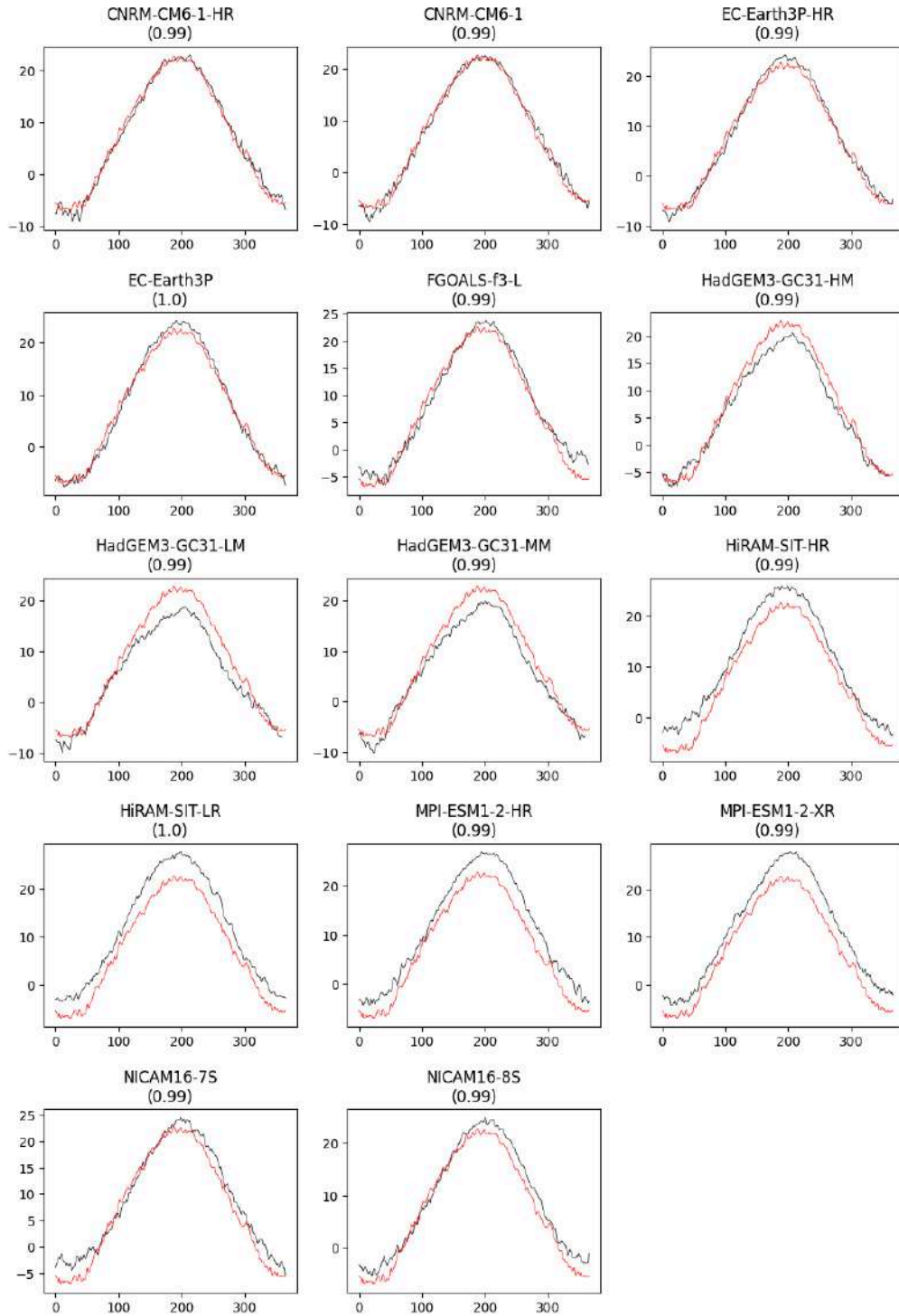
### Seasonal cycle of tasmax



Figures in brackets are correlation between model vs. MSWX

Figure A.12: Seasonal cycles of daily maximum temperatures in observations (MSWX), shown in black, and HighResMIP models, shown in red.

Seasonal cycle of tasmin



Figures in brackets are correlation between model vs. MSWX

Figure A.13: Seasonal cycles of daily minimum temperatures in observations (MSWX), shown in black, and HighResMIP models, shown in red.